J. Fluid Mech. (1985), *vol.* 157, *pp.* 163–197
Printed in Great Britain

On the structure of jets in a crossflow

By J. ANDREOPOULOS†
Gas Dynamics Laboratory, Department of Mechanical and Aerospace Engineering, Princeton University, Princeton, NJ 08544

(Received 2 December 1983 and in revised form 27 September 1984)

Spectral analysis and flow visualization are presented for various velocity ratios and Reynolds numbers of a jet issuing perpendicularly from a developing pipe flow into a crossflow. The results are complete with conditional averages of various turbulent quantities for one jet-to-cross-flow velocity ratio R of 0.5. A unique conditional-sampling technique separated the contributions from the turbulent jet flow, the irrotational jet flow, the turbulent crossflow and the irrotational crossflow by using two conditioning functions simultaneously. The intermittency factor profiles indicate that irrotational cross-flow intrudes into the pipe but does not contribute to the average turbulent quantities, while the jet-pipe irrotational flow contributes significantly to them in the region above the exit where the interaction between the boundary-layer eddies and those of the pipe starts to take place. Further downstream, the contributions of the oncoming boundary-layer eddies to the statistical averages reduce significantly. The downstream development depends mainly on the average relative eddy sizes of the interacting turbulent fields.

1. Introduction

This paper is one of a series describing a jet-in-a-crossflow experiment carried out at the SFB 80 of the University of Karlsruhe. The experimental program included: (1) a detailed flow-visualization study reported by Foss (1980); (2) wall-static-pressure measurements reported by Andreopoulos (1982); and (3) mean- and fluctuating-velocity and temperature measurements reported by Andreopoulos & Rodi (1984) and Andreopoulos (1983*b*).

The present paper describes some structural characteristics of the flow, additional to those observed by Foss, and an attempt is made to illuminate the way the crossflow boundary layer mixes and/or interacts with the jet-pipe flow (see figure 1). In cases where the jet velocity V_j is much higher than the cross-stream velocity U_e, the near field is controlled largely by complex inviscid dynamics so that the influence of turbulence on the flow development is rather limited. However, the flow downstream is always influenced by turbulence and at small velocity ratios R, where $R = V_j/U_e$, even the near field is turbulence dominated. The aim of the present investigation is to increase the physical understanding of the turbulence processes which are involved in the case where the initial jet layer interacts with the oncoming crossflow boundary layer and where the turbulence is subjected to extra rates of strain such as those resulting from streamwise curvature, lateral divergence and longitudinal accelerations.

Section 2 briefly describes the experimental arrangement and the data reduction procedures. A unique conditional-sampling technique which uses two conditioning

† Formerly at the Sonderforschungsbereich 80, University of Karlsruhe, F.R.Germany.

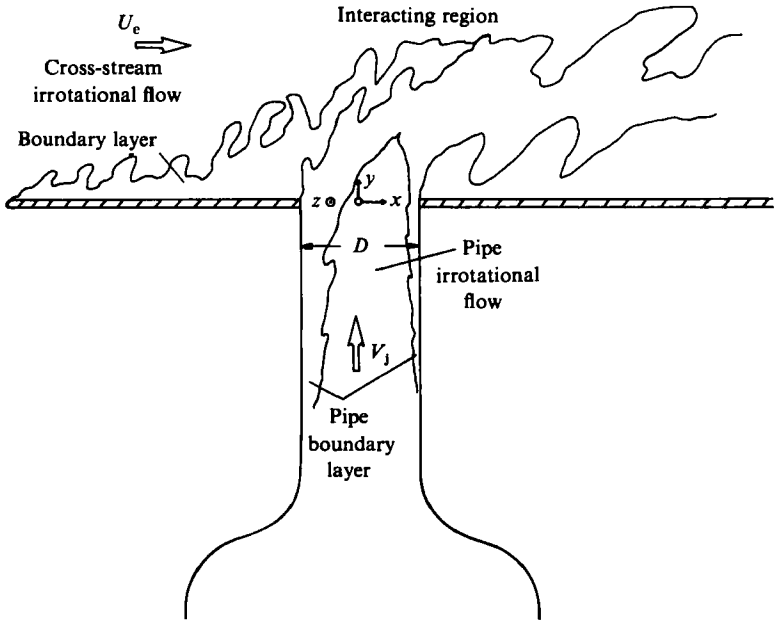

FIGURE 1. Flow configuration with interacting shear layers.

functions simultaneously is also described. In §3 a selection of the results are presented and discussed. The main conclusion of the present work is that the flow in the interaction region 'time shares' between four possible zones, namely irrotational cross-stream flow, irrotational pipe flow, turbulent boundary layer flow (which develops over the flat plate), and turbulent pipe flow. The existence of large structures in the jet which are rather well organized at low Reynolds number is also described and discussed.

2. Experimental techniques

2.1. *Experimental set-up*

The measurements were made in the closed-circuit wind tunnel at the Sonderforschungsbereich 80. The experimental set-up is fully described by Andreopoulos (1982). The pipe diameter D was 50 mm and the pipe length, from the plenum to the jet exit, was $12D$. Both interacting flow fields, i.e. the pipe flow and the crossflow, were found to be developing turbulent flows for all the velocity ratios investigated. At four diameters upstream of the jet exit, on the plate, where the jet interference on the cross-stream was negligible, a friction coefficient $C_f = 0.0037$ and a boundary-layer thickness of $\delta = 0.278D$ were measured at a free-stream velocity of $U_e = 13.9$ m/s. Velocity signals were obtained with a DISA X-wire probe type P51 and analysed using a Hewlett-Packard Fourier Analyser 5154C with four Analog to Digital Converters of 12 bits per word resolution. Such a probe gives good results if the data-analysis technique accounts for the high pitch and yaw angle of the instantaneous velocity vector. As was mentioned by Andreopoulos & Rodi (1984), the present flow configuration includes regions with reasonably high turbulence levels and therefore the response of the hot wire at high pitch or yaw angles should be known. Hence, the algorithm proposed by Andreopoulos (1981) was adopted to reduce the data.

For the spectral analysis each of the cross-wire channels was passed to two analog-to-digital converters (ADC); one to yield the mean value of the input voltage and the other to calculate the fluctuating quantities. This arrangement allowed the whole dynamic range of the ADC to be used and a resolution of 0.24 mv/word was achieved. The cutoff frequency of the AC mode input was about 0.3 Hz. All inputs were low-pass filtered at 10 kHz and digitized at 25 kHz per channel.

The jet flow was visualized by introducing a fog of paraffin oil droplets into the plenum chamber through a row of holes on a tube spanning the chamber width. The overpressure used was small enough to ensure laminar flow. Because the tunnel walls were opaque, a mirror was installed inside the wind tunnel to allow the flow to be photographed. The photographic records were obtained with a NIKON motor-driven camera and the film used was ASA 800 with a $\frac{1}{1000}$ s exposure time.

2.2. *Conditional-sampling techniques*

Many investigations of turbulent shear flows have used the technique of conditional sampling to provide more information about regions of interest in these flows. Antonia (1981) describes the various existing conditional-sampling techniques and points out that probably the most plausible way to investigate the interaction of *two*, initially separate, turbulent fields is to use temperature as a passive marker of *one* of the interacting fields, an idea of Bradshaw's (1975). This 'tagging' of the flow allows a distinction to be made between 'hot-zone' and 'cold-zone' contributions. In the present case, it was decided to slightly heat the jet-pipe flow by means of heating elements located before the plenum chamber at the exit of the two-stage compressor which supplied the pipe flow.

The part of the pipe which was inside the wind tunnel and underneath the flat plate was carefully insulated to avoid additional heat transfer by conduction and convection. In this way, the jet flow was heated a few degrees above the ambient cross-stream temperature, and any asymmetry in the temperature profiles can be attributed to the crossflow and not to cooling of the pipe by the wind-tunnel flow. This asymmetry was detected for 3–4 diameters before the pipe exit. Further down, deep inside the pipe, both mean- and fluctuating-temperature profiles were found to be quite flat, demonstrating the homogeneity of the temperature distribution in the pipe.

Turbulence measurements were made using DISA type 55M01-anemometers and type 55P51 miniature cross-wire probes. In addition a 1 μm 'cold wire' was mounted on a home-made probe clamped to the side of the cross-wire probe. The cold wire was operated by a constant-current home-made circuit with a heating current of 0.2 mA. The papers by LaRue, Denton & Gibson (1979), Lecordier, Paranthoen & Petit (1982) and Perry, Smits & Chong (1975) give some more details of the way which the sensor parameters affect its performance. Because of its low-frequency response, the cold-wire output was compensated in real time by a conventional operational-amplifier network. The compensation was adjusted to obtain the sharpest possible rise and fall of the temperature signal at the leading and trailing edges of bursts of hot fluid, while avoiding an 'over-shoot' of temperature below the free-stream value. The techniques associated with the temperature fluctuations are similar to those described in the wake study of Andreopoulos & Bradshaw (1980).

The data-reduction scheme used was similar to that described in §2.1. The signals were digitized at 5 kHz per channel and stored on digital magnetic tapes for later data reduction. To increase the accuracy of the measurements, the probe was carefully aligned parallel to the mean flow.

The earliest known applications of conditional sampling were by Townsend (1949)

and Corrsin & Kistler (1955). Since then, the technique has been further developed and used by many research workers. Most of them have used either *temperature-conditioning* sampling (Dean & Bradshaw 1976; LaRue & Libby 1974; Antonia, Prabhu & Stephenson 1975; Sreenivasan, Antonia & Stephenson 1978; Chen & Blackwelder 1978; Fabris 1979) or *velocity-conditioning* sampling (Fiedler & Head 1966; Kovasznay, Kibens & Blackwelder 1970; Hedley & Keffer 1974; Paizis & Schwarz 1974; Oswald & Kibens 1971; Gutmark & Wygnanski, 1976; Wygnanski & Fiedler 1970; Jenkins & Goldschmidt 1976; Chevray & Tutu, 1978). Muck (1980) and Murlis, Tsai & Bradshaw (1982) compared the two schemes of conditioning and used both, one independent of the other, to investigate low-Reynolds-number effects in boundary layers. The present approach couples the two schemes together in a unique way which can yield complementary information on the interaction of the two turbulent fields.

The conditional-sampling algorithm is similar in principle to that used by Andreopoulos & Bradshaw (1980) and is fully described by Weir, Wood & Bradshaw (1981). Fluid is labelled 'hot', i.e. jet fluid, if its temperature exceeds a certain threshold value, usually around 0.1 °C. To distinguish the end and the beginning of hot periods as sharply as possible, data points are also labelled 'hot' if the time derivative of the temperature exceeds a certain small value. As was previously explained and also clearly shown in figure 1, the heated jet flow is a developing turbulent flow, i.e. significant regions of potential core are present in addition to the turbulent-flow regions. Similarly, the unheated boundary-layer flow entrains cross-stream potential flow. It is also expected that the irrotational-fluid fluctuations of both flow fields will contribute to the conventional mean quantities. In the light of the unsteady character of the jet, these contributions may be significant. It is therefore necessary to further discriminate the flow into turbulent and non-turbulent fluid. In this case fluid labelled as 'hot' *and* 'turbulent' belongs to a jet-flow eddy while 'cold' *and* 'turbulent' fluid is part of an eddy of the flat-plate boundary-layer flow. Fluid that is labelled as 'hot' *and* 'non-turbulent' or 'cold' *and* 'non-turbulent' comes from the jet irrotational flow or cross-stream irrotational flow, respectively.

The conditional-sampling algorithm discriminates firstly between the hot/cold fluid and subsequently the turbulent/non-turbulent fluid. The temperature serves as the 'conditioning function' in the former discrimination. The uv-signal is used in the latter case of turbulent/non-turbulent discrimination, mainly because uv is directly involved in the production of turbulence, since $\overline{uv}$ is the main shearing stress (see Andreopoulos & Rodi 1984).

The advantages of using the uv-signal in conditional measurements have been aptly noted by Wallace, Eckelman & Brodkey (1972) and Willmarth & Lu (1972) and extensively discussed by Murlis *et al.* (1982) and Muck (1980). If the time derivative of the instantaneous uv-signal is above a prescribed threshold value, the fluid is described as turbulent. The second derivative of the uv-signal is also used as back-up criterion. According to the above discussion the following definitions have been made for the intermittency functions I_θ and I_{uv} of the hot/cold and turbulent/non-turbulent fluid, respectively:

$$I_\theta = \begin{cases} 1 & \text{if } T \geqslant \theta_1 \quad \text{and/or} \quad \dfrac{\partial T}{\partial t} \geqslant \theta_2 \\ 0 & \text{otherwise,} \end{cases}$$

and

$$I_{uv} = \begin{cases} 1 & \text{if } \dfrac{\partial uv}{\partial t} \geqslant \theta_3 \quad \text{and/or} \quad \dfrac{\partial^2 uv}{\partial t^2} \geqslant \theta_4 \\ 0 & \text{otherwise.} \end{cases}$$

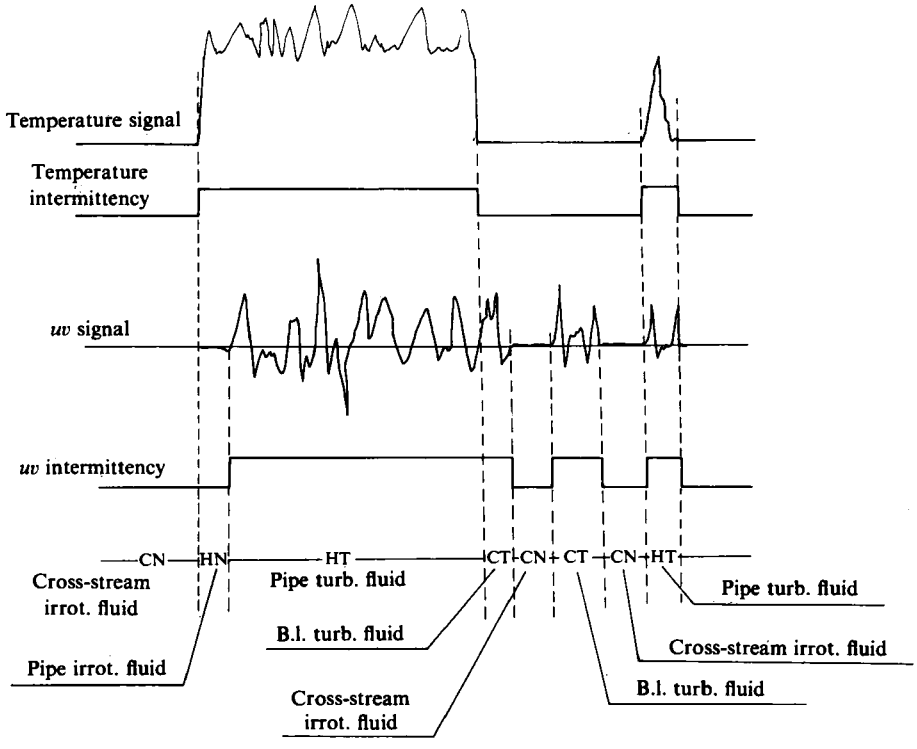

FIGURE 2. Deduction of Cold and Non-turbulent (CN), Hot and Non-turbulent (HN), Cold and Turbulent (CT) and Hot and Turbulent (HT) zones from *uv* and temperature signals.

Figure 2 shows highly idealized temperature and *uv*-traces somewhere in the interaction region, above the exit plane of the jet. It is obvious that the beginning and the end of a 'hot' burst may not correspond with the beginning and the end of turbulent activities shown in the *uv*-signal. This difference cannot be attributed to problems of the spatial resolution of the probe; even with the 'cold-wire' 1 mm ahead of the cross-wire the difference in arrival time is not more than one digitization interval. It is also clear in this idealized figure that turbulent activities shown in *uv*-traces may not correspond to any temperature excursion. The output of the hot/cold discrimination part of the algorithm corresponding to the temperature trace of the figure is shown immediately below it. The output of the turbulent/non-turbulent discrimination part of the algorithm corresponding to the *uv*-trace is shown below it. Combination of both parts of the algorithm yields the final discrimination shown at the bottom part of the figure. The suffix C is used to indicate Cold fluid, i.e. crossflow, the suffix H is used to indicate Hot fluid, pipe flow, the suffix T is used to indicate Turbulent fluid and finally N is used to indicate irrotational fluid regardless of whether it is pipe-jet or cross-stream flow. Two suffixes are needed to fully describe the flow. HT indicates Hot *and* Turbulent fluid, i.e. turbulent-pipe fluid, CT indicates Cold *and* Turbulent fluid, i.e. flat-plate boundary-layer fluid, HN indicates Hot and Non-turbulent fluid, i.e. irrotational pipe flow, and CN indicates Cold and Non-turbulent fluid, i.e. irrotational cross-stream flow.

The results presented here measure all fluctuations with respect to the conventional-average velocity. The conditional-average products of velocity fluctuations can be presented as contributions of the above-mentioned zones to the conventional average.

If Q is any velocity fluctuation product of the form $u^m v^n$, with m, n integers, then the contributions of the four zones are defined as follows:

$$\bar{Q}_{\mathrm{HT}} = \lim_{T\to\infty}\left[\frac{1}{T}\int_{t_0}^{t_0+T} Q(X,t)\, I_\theta(X,t)\, I_{uv}(X,t)\,\mathrm{d}t\right],$$

$$\bar{Q}_{\mathrm{CT}} = \lim_{T\to\infty}\left[\frac{1}{T}\int_{t_0}^{t_0+T} Q(X,t)\,[1-I_\theta(X,t)]\, I_{uv}(X,t)\,\mathrm{d}t\right],$$

$$\bar{Q}_{\mathrm{CN}} = \lim_{T\to\infty}\frac{1}{T}\int_{t_0}^{t_0+T} Q(X,t)\,[1-I_\theta(X,t)]\,[1-I_{uv}(X,t)]\,\mathrm{d}t\Big],$$

$$\bar{Q}_{\mathrm{HN}} = \lim_{T\to\infty}\left[\frac{1}{T}\int_{t_0}^{t_0+T} Q(X,t)\, I_\theta(X,t)\,[1-I_{uv}(X,t)]\,\mathrm{d}t\right],$$

with the conventional average

$$\bar{Q} = \lim_{T\to\infty}\left[\frac{1}{T}\int_{t_0}^{t_0+T} Q(X,t)\,\mathrm{d}t\right].$$

After these definitions, the zone contributions sum to give the conventional average,

$$\bar{Q}_{\mathrm{HN}}+\bar{Q}_{\mathrm{CN}}+\bar{Q}_{\mathrm{HT}}+\bar{Q}_{\mathrm{CT}} = \bar{Q}, \tag{1}$$

as suggested by Dean & Bradshaw (1976).

If γ is the mean value of the intermittency function $I(t)$, hereafter simply called intermittency, then the zone average $\tilde{Q}$ is related to the zone contributions as follows:

$$\tilde{Q}_{\mathrm{HT}} = \frac{\bar{Q}_{\mathrm{HT}}}{\gamma_{\mathrm{HT}}},\quad \tilde{Q}_{\mathrm{CT}} = \frac{\bar{Q}_{\mathrm{CT}}}{\gamma_{\mathrm{CT}}},\quad \tilde{Q}_{\mathrm{HN}} = \frac{\bar{Q}_{\mathrm{HN}}}{\gamma_{\mathrm{HN}}},\quad \tilde{Q}_{\mathrm{CN}} = \frac{\bar{Q}_{\mathrm{CN}}}{\gamma_{\mathrm{CN}}}.$$

In the present work the discrimination scheme of 'retail' intermittency has been employed (see Bradshaw & Murlis 1974) without explicit application of any 'hold time' other than digital-sampling time. This scheme is believed to follow more closely the highly re-entrant nature of the interface which is clearly shown in the smoke pictures. Although the intermittency measurement itself depends on the length and the number of the irrotational 'drop-outs' (see LaRue & Libby 1974; Murlis *et al.* 1982; Muck 1980), the zone contributions to the fluctuation statistics are much less dependent on the drop-outs. The present intermittency scheme has been applied and tested in the case of a partially heated boundary-layer flow with satisfactory results. Small differences, of the order of a few percent, between the two discrimination schemes were found, but the effect of the conditional averages was negligible. Therefore any significant difference in the zonal contributions to Q in (1) are genuine and are *not* caused by relatively small errors in intermittency. Following the suggestions of Muck (1980) the thresholds θ_3 and θ_4 which are used in the turbulent/non-turbulent discrimination are directly connected to the averages of the derivatives of the uv signal in the turbulent zone, $\widetilde{\partial uv/\partial t}$ and $\widetilde{\partial^2 uv/\partial t^2}$ respectively, that is, the thresholds were continually updated. Similarly the 'cold fluid temperature level' T was continually updated in the temperature-intermittency scheme. It is emphasized here that the thresholds for the uv-derivative scheme are not necessarily the same for both turbulent zones:

$$\theta_{3\mathrm{C}} = C_{3\mathrm{C}}\left|\widetilde{\frac{\partial uv}{\partial t}}\right|_{\mathrm{CT}},\quad \theta_{4\mathrm{C}} = C_{4\mathrm{C}}\left|\widetilde{\frac{\partial^2 uv}{\partial t^2}}\right|_{\mathrm{CT}},$$

$$\theta_{3\mathrm{H}} = C_{3\mathrm{H}}\left|\widetilde{\frac{\partial uv}{\partial t}}\right|_{\mathrm{HT}},\quad \theta_{4\mathrm{H}} = C_{4\mathrm{H}}\left|\widetilde{\frac{\partial^2 uv}{\partial^2 t}}\right|_{\mathrm{HT}},$$

where C_{3C}, C_{4C}, C_{3H} and C_{4H} are constants. The values of the constants have been so optimized as to give minimum dependence of the results on these values. In the present investigation, the optimum values were found to be $C_{3C} = 0.2$, $C_{3H} = 0.28$, $C_{4C} = 0.22$ and $C_{4H} = 0.29$. Thus, the present procedure is self adjusting and allows cases to be handled where the lengthscale of one turbulent zone differs from that of the other.

Some typical features of the present scheme are shown in figures 3(*a*), (*b*), and (*c*) which show the temperature trace, the u- and v-component velocity traces and the intermittency-function signal. For the purpose of demonstration, the intermittency has values 1.5, 1.0, 0.5 and 0, corresponding to the HT, CT, HN and CN zones respectively. The traces shown in figure 3(*a*) were obtained four diameters downstream on the plane of symmetry $z/D = 0$, at a normal distance $y/D = 1$. The temperature fluctuations are of the order of 1 °C, and most of the fluid in that record is considered as 'hot', with some exceptions, indicated by arrows on the temperature trace, where the fluid is determined as cold. The highly intermittent character of the turbulent/non-turbulent interface is also shown in the uv-trace, where extremely high fluctuations, of the order of 0.16 U_e^2, are observed. The traces on figure 3(*b*) were taken at the same downstream location $x/D = 4$, but at a higher distance from the wall, well inside the crossflow free stream where the temperature fluctuations are small. As the vertical scale of the temperature trace shows, the temperature fluctuations are very small, sometimes of the order of the noise level. There are indeed four temperature excursions which can be regarded as genuine temperature fluctuations and indicated by arrows on the figure. The threshold must be set above the 'noise level' which, as can be shown from the trace, is about 0.17 °C and includes the electronic noise as well as the unavoidable velocity fluctuations on the 'cold' wire. True temperature fluctuations with an amplitude smaller than the threshold level, like that at 0.07 time units, cannot therefore be detected by the algorithm. It is also very interesting to see the irrotational fluctuations on the u- and v-velocity component traces. As the large-scale structures travel downstream, they induce velocity fluctuations in the irrotational fluid, particularly in the free stream of the crossflow. Some of these fluctuations are not evident at all in the uv-trace, as shown by the arrows in the first half of the total time-record length, and consequently are not detected as turbulent by the algorithm. In the second half of the time record there are irrotational fluctuations on the uv-traces but again not detected as turbulent. It is therefore clear from this example that irrotational fluctuations in the cross-stream can be included in the CN zone, as they must be. As can be shown later, the contributions of this zone to the average turbulent quantities may not be negligible.

Figure 3(*c*) demonstrates a case where the threshold of temperature gradient detection has been activated to pick up the short cold-fluid excursions inside a hot fluid. In most of the cases, these fluctuations have been detected correctly since this back-up criterion gives a 'turbulence-retail' character to the scheme in the sense used by Murlis *et al.* (1982). About 10% of the total length of each of the data records obtained have been plotted in the way presented in figure 3 and inspected by eye to check that the discrimination schemes behaved satisfactorily.

3. Results

3.1. *Spectral analysis*

Figure 4 shows some typical u- and v-spectra obtained at three different measuring points on the jet-exit plane at $R = 0.25$. The annular pipe boundary layer did not, because of strong variation of the pressure gradient around the exit, have a constant

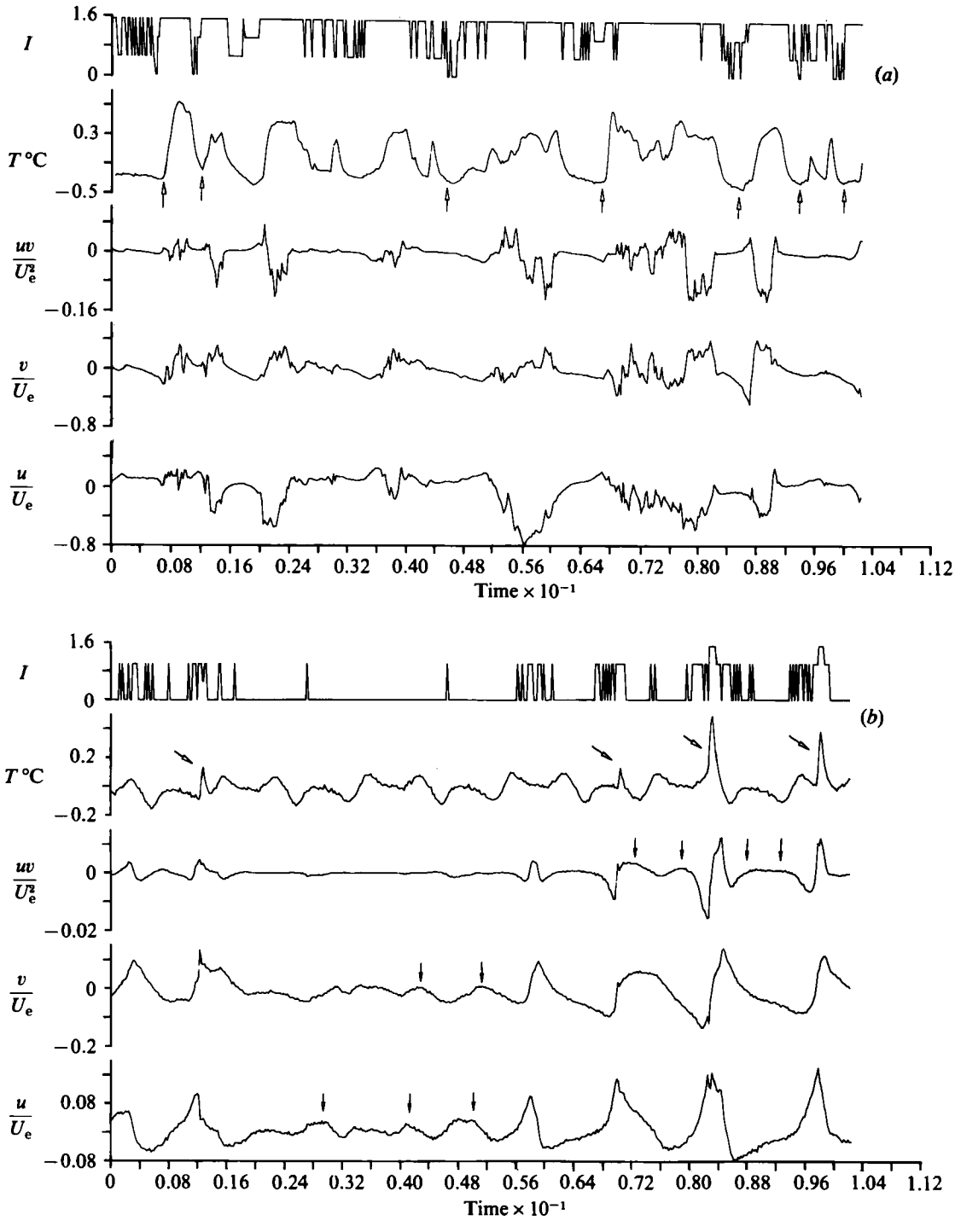

FIGURE 3(*a*, *b*). For caption see opposite page.

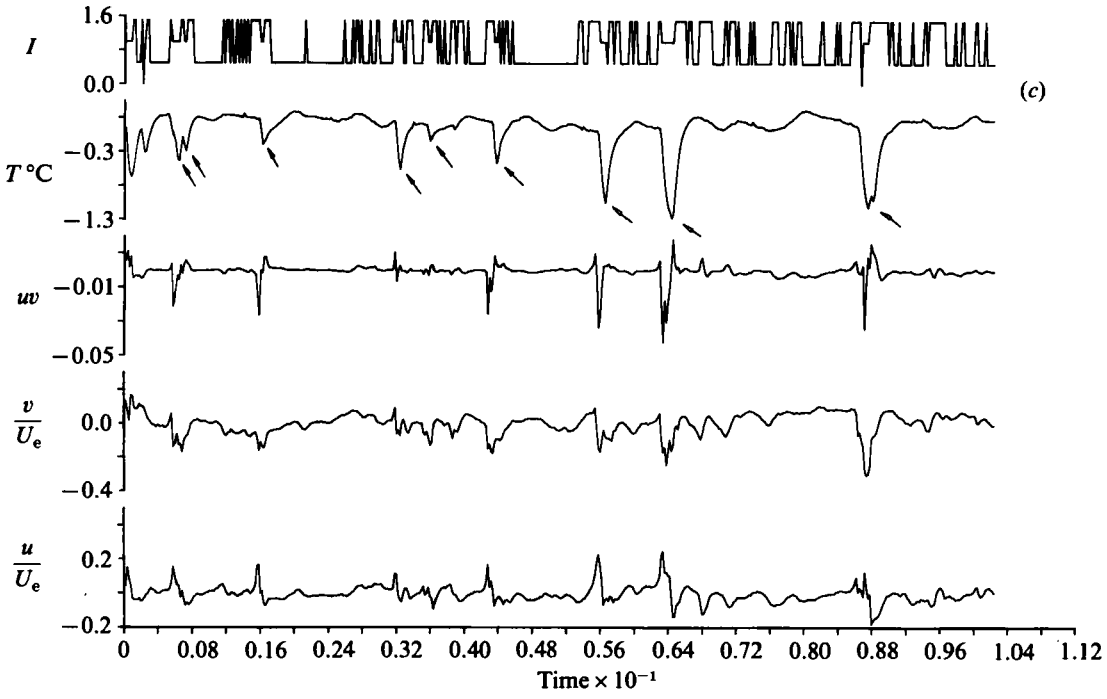

FIGURE 3. Typical examples of T, uv, u and v signals with the corresponding combined intermittency functions which can take values 1.5, 1.0, 0.5, and 0.0 for the HT, CT, HN and CN zones respectively: (*a*) at $x/D = 4$ and $y/D = 1$; (*b*) 4 and 1.3; (*c*) 0.5 and 0.4. The vertical scale in the temperature trace is in °C and the timescale in tenths of second.

thickness around the circumference; near the upstream edge of the pipe its thickness was roughly $0.55D$ ($D = 50$ mm) and it reduced gradually around the exit before reaching a value of $0.2D$ at the downstream edge of the pipe. These values were deduced from the shear-stress profiles, as it is usually done in cases with strong pressure gradients where the mean-velocity distribution is not uniform. These spectra were obtained in each of the three characteristic regions at the exit. The first station at $x/D = -0.35$ is inside the annular pipe boundary layer which is developing near the upstream edge of the pipe under the influence of an adverse pressure gradient. The second measuring point lies very close to the pipe axis where the flow has a rather intermittent behaviour between turbulent and non-turbulent fluid with rather small turbulence intensity. The last point at $x/D = +0.40$ is close to the downstream edge of the pipe where the flow is developing under the influence of a favourable pressure gradient. The peak frequency at 108 Hz shown in figure 4 was also evident in the autocorrelation plots, but it is more pronounced at $x/D = +0.4$ and less at $x/D = -0.35$. The same peak frequency was observed at stations farther downstream, at y positions just outside the turbulence region, as well as at different velocity ratios R. It was, however, found that this frequency was independent of the y and z positions. Figure 5(*a*) shows the Strouhal number variation as function of the downstream distance x at different velocity ratios R. The Strouhal number was defined as $St = fD/U_e$ where f was the peak frequency, U_e the cross-stream velocity, which was kept constant during these experiments with different R, and D the pipe diameter. Some frequency halving was also observed and its implication will be discussed later on in this section. The data at different R and x collapse reasonably

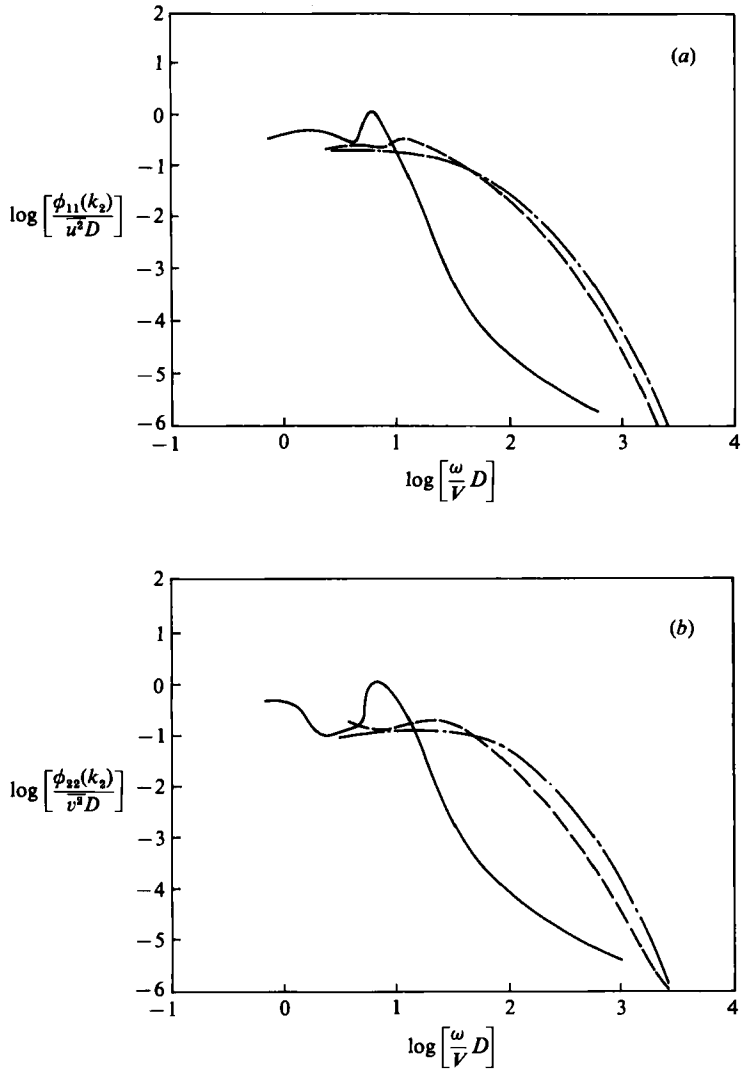

FIGURE 4. (*a*) Power spectrum of u fluctuation. (*b*) Power spectrum of v-fluctuation at the jet exit for $R = 0.25$: —, $x/D = 0.40$; ----, -0.14; —·—, -0.35.

together to $St = 0.41$, a value which seems to be independent of the Reynolds number based on the jet velocity, $Re = V_j D/\nu$, (figure 5*b*), at least in the range investigated here. The reader is reminded that the existing pipe flow changes significantly with R (see Foss 1980; Andreopoulos 1982). This result suggests that the Strouhal number is associated with puffing or vortex-ring roll up, or some mechanism associated largely with the change from pipe to jet flow. In fact these measurements agree quite well with the measurements of Yule (1978) in the turbulent regime of a round jet issuing into 'still' air which are plotted in figure 5(*b*). Similar observations have been made by Bradbury & Khadem (1975) in their investigation of jets distorted by tabs. They reported a value of $St = 0.45$ at $Re = 6 \times 10^5$. In the case of round jets issuing into 'still' air the Strouhal number is defined as $St = fD/V_j$. Thus, a direct comparison with the present results is possible only in cases where $U_e = V_j$, i.e. $R = 1$. The agreement of the measured Strouhal number between the present flow with $R = 1$

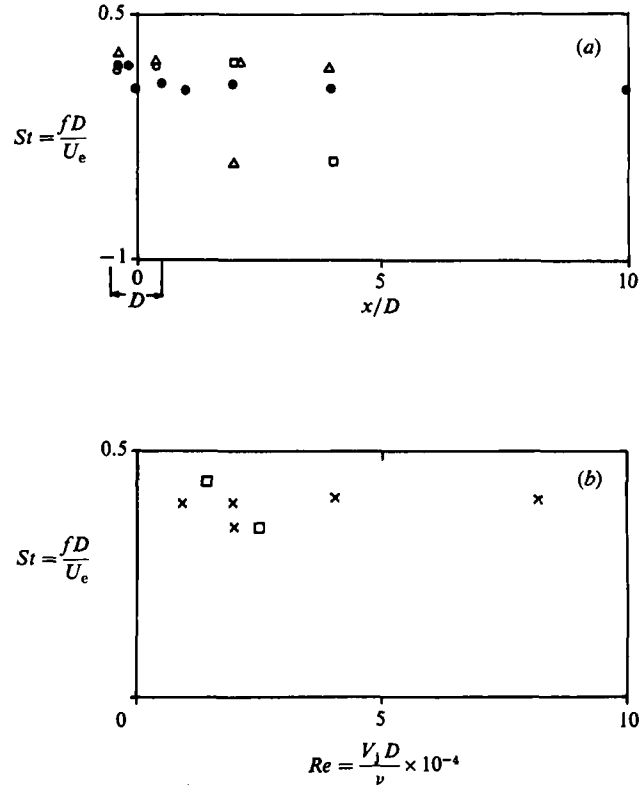

FIGURE 5. (*a*) Strouhal number $St = fD/U_e$ at various downstream positions. ○, $R = 0.25$; ●, 0.5; △, 1; □, 2. (*b*) Strouhal number versus $Re = V_j D/\nu$ at constant $Re = U_e D/\nu = 4.1 \times 10^4$; □ Yule (1978).

and that of axisymmetric jets at zero crossflow ($U_e = 0$) shows that the jet retains *some* of its characteristics, even in the presence of a crossflow ($U_e \neq 0$).

As previously documented (Yule 1978; Crow & Champagne 1971) the free-jet flow depends strongly on Reynolds number and the initial conditions, and it can undergo various kinds of instabilities, which cause the rolling up of the annular mixing layer and the formation of toroidal vortices. These vortices, or vortical rings, as they travel downstream, can undergo successive interactions like pairing and tearing. This might explain the observed frequency peak and frequency halving. Vortex shedding, however, might be another explanation, since it has been reported previously (see McMahon, Hester & Palfery 1971) that such shedding takes place at very high velocity ratios. In these cases, the jet penetrates very deeply inside the crossflow before it starts to bend over and therefore behaves a little like a rigid cylinder. In the present case, however, the jet penetrates no more than 2 diameters into the crossflow. Therefore it seems quite unlikely that vortex shedding, in the strict sense of shedding of Ω_y vorticity, takes place at the smaller velocity ratios. Apart from that, if shedding of Ω_y vorticity was happening, the frequency at the plane of symmetry should be double that measured at a position far outside the plane of symmetry. In fact, by moving the hot-wire probe on a plane perpendicular to the x-axis, no variations in frequency were observed. There are two other possible explanations of the observed frequency peak, namely 'puffing' of the jet or some sort of 'flapping'. The first could be owing to an unsteady operation of the two-stage

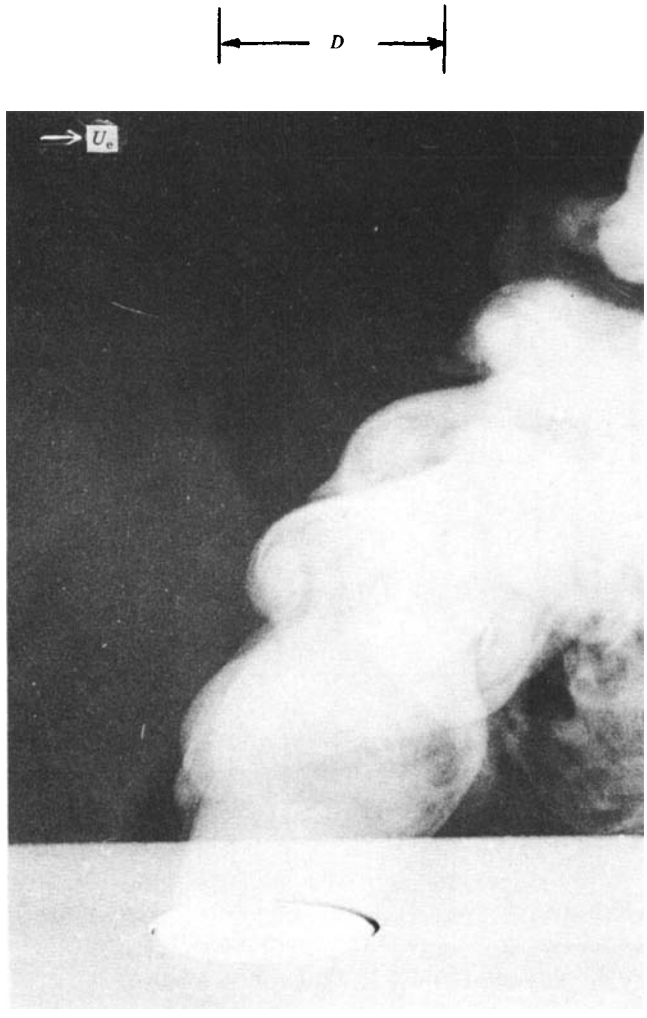

FIGURE 6. Flow visualization of rolling up of the shear layer. $R \approx 4$, $Re \simeq 5.1 \times 10^3$, $D = 0.08$ m, $V_j = 1$ m/s, $U_e = 0.25$ m/s.

blower supplying the jet flow. However, no frequency peaks were observed at a position half a diameter upstream inside the pipe, and therefore puffing due to a blower unsteadiness does not appear to occur.

'Flapping' is known to take place in plane jets (Goldschmidt & Bradshaw, 1973) but nothing similar has been reported for the jet into a crossflow. It is therefore unlikely to be the cause of the periodic motion present in this experiment. In fact two cross-wires placed at opposite sides of the jet in the z-direction showed that the U-velocity components were in phase while the W-velocity components were in antiphase. This indicates that the frequency peaks are most probably due to the sequential shedding of large structures.

3.2. *Flow visualization*

The present flow depends strongly on initial conditions and/or Reynolds number. Therefore the flow visualization covers different Reynolds numbers and a range of velocity ratios from $R = 4$ to $R = 0.25$. Although the smoke was not finely controlled

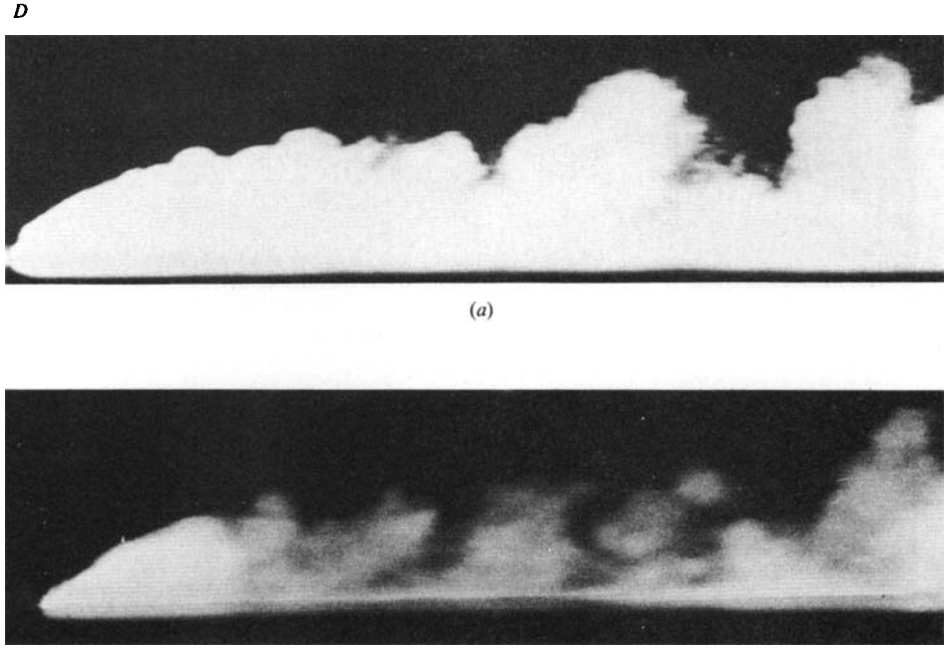

FIGURE 7. Flow visualization with $R = 1$, $D = 0.05$ m: (*a*) $Re = 2 \times 10^4$; (*b*) 8.3×10^4.

and the photos show a flow picture averaged along the light path normal to the paper, the flow-visualization study was extremely useful in confirming the existence of large structures in the flow and in revealing some more details of their behaviour.

Figure 6 demonstrates a rolling up of the shear layer, particularly evident in the upstream boundary of the jet, where the velocity ratio was relatively high, $R = 4$, and the Reynolds number $Re = V_j/D\nu = 5 \times 10^3$. This rolling up, also observed by Foss (1980), starts to take place at about $1D$ above the exit and persists to about $4D$ downstream along the jet path. The vortical rings so formed carry vorticity of the same sign as the flow inside the pipe and are, with respect to the jet axis, subjected to asymmetrical stretching, transport and tilting due to the crossflow. For example, the windward side of the jet is decelerated with respect to the lee side in the very near field and this results in a stretching of the vortex lines. Further downstream, and in particular after the bending over of the jet, the upper side of the jet is accelerated with respect to the lower side, resulting in a compression of vortex lines. Strictly speaking, this is a hypothetical case because the vortical rings break down to turbulence during or before the bending over. Such vortical rings are formed only at low Reynolds numbers, and high velocity ratio R, with laminar flow inside the pipe. These flow conditions characterized the case of the flow shown in figure 6, where the unavoidable natural disturbances did not drive the flow to turbulence, as opposed to the flow cases shown in figures 7–9 where the flow was tripped at a distance of $12D$ from the exit inside the pipe. Since the development distance of $12D$ was not long enough, the flow at the exit was not fully developed turbulent flow.

Figures 7–9 show some pictures of the downstream development of the flow at various velocity ratios and Reynolds numbers. Figure 7 shows visualization of the flow with velocity ratio $R = 1$ at Reynolds numbers of 2×10^4 (figure 7*a*) and $Re = 8.3 \times 10^4$ (figure 7*b*). Figure 8 shows pictures of a flow with $R = 0.5$ at three different Reynolds numbers: 2×10^4 (figure 8*a*), 4.1×10^4 (figure 8*b*) and 8.3×10^4

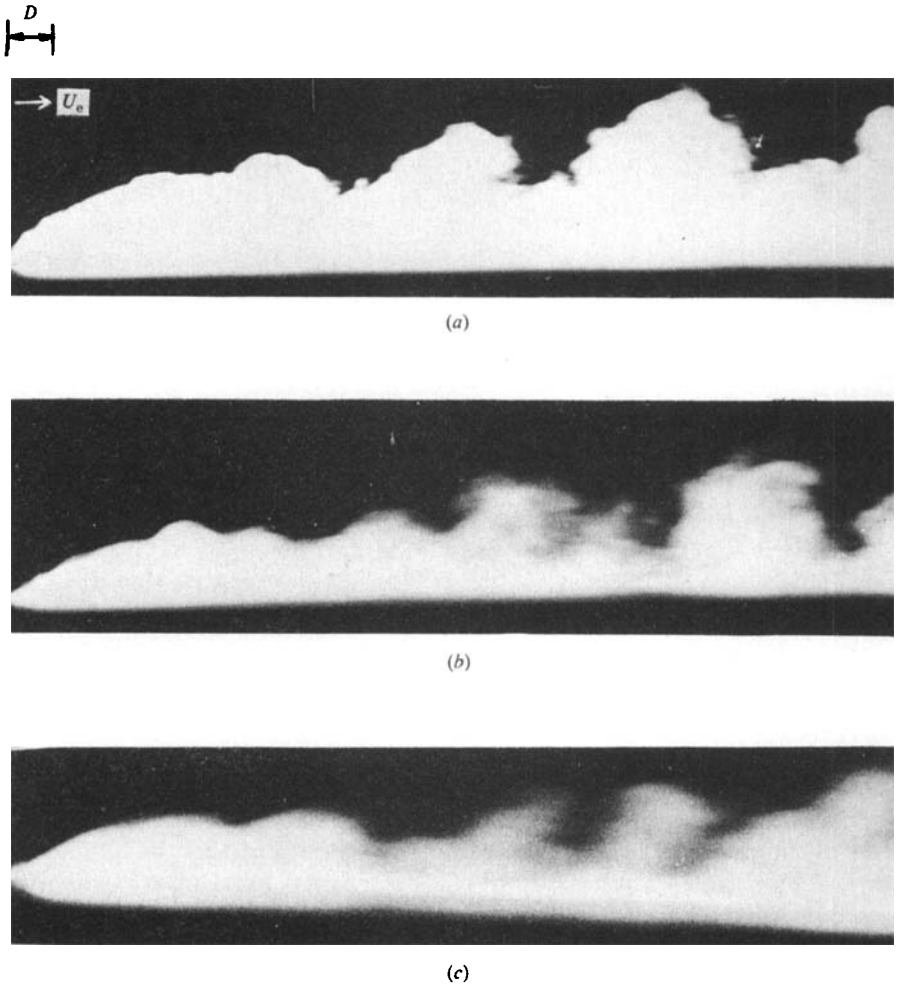

FIGURE 8. Flow visualization with $R = 0.5$, $D = 0.05$ m: (a) $re = 2 \times 10^4$; (b) 4.1×10^4; (c) 8.3×10^4.

(figure 8c). Finally figure 9 shows two pictures of the flow with $R = 0.25$ at two Reynolds numbers, 4.1×10^3 and 8.3×10^4. One common feature of all pictures is the diffuse appearance of the smoke in the flow field close to the jet exit where the flow scales are very small, but there is a sharp convoluted interface in the outer layer. At higher Reynolds numbers, high concentration gradients are evident very close to the wall at all velocity ratios investigated. However, the main characteristic of all the cases at low Reynolds numbers is the regular appearance of large-scale structures with some coherence in their behaviour. These structures emanate from the pipe regularly, carrying a vorticity with the same sign as the pipe eddies and having a size of the order of the annular pipe boundary-layer thickness. This thickness depends primarily on the Reynolds number of the pipe flow, but it is always less than $1D$. It must be emphasized here that the vorticity of these structures is *opposite* in sign from the vorticity carried by the cross-stream boundary layer. However, it is reoriented, stretched and finally, within a short distance of roughly 6–10 D, diffused by the action

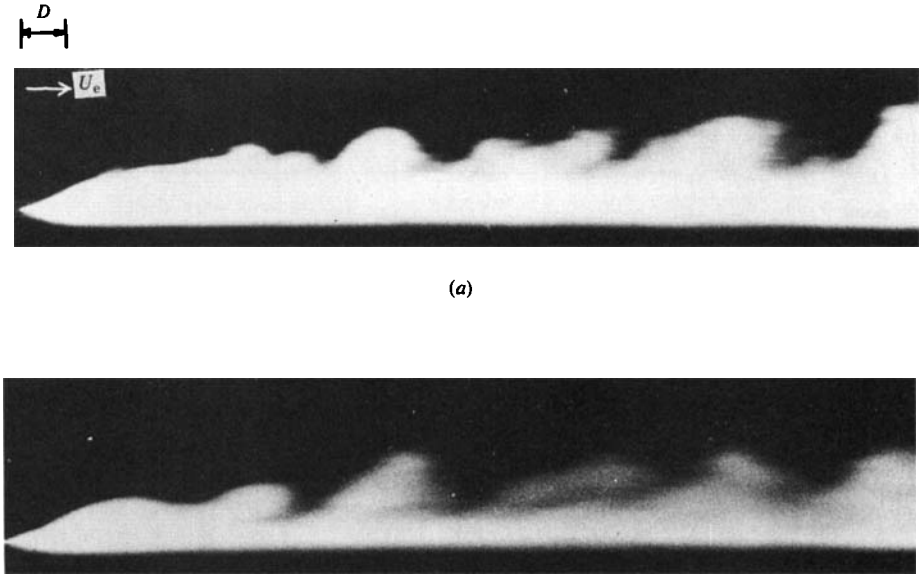

FIGURE 9. Flow visualization with $R = 0.25$, $D = 0.05$ m: (*a*) $Re = 4.1 \times 10^4$; (*b*) 8.3×10^4.

of the turbulent shear stresses and viscosity. At that point eddies with opposite vorticity start to appear, i.e. with sign like that of the cross-stream boundary-layer eddies. It seems that in this down-stream region the solid wall begins to dominate the flow, and imparts some boundary-layer characteristics, like the sign of the carried vorticity $\partial U/\partial y$. As the Reynolds number increases, the regularity of appearance of the large structures originating at the pipe decreases and these structures begin to occupy a rather wide range of sizes. The downstream structures are larger in size, of the order of 2–3D, and can grow in size by pairing as the halving of the frequency, shown in figure 5(*a*), suggests. Another significant feature of the flow is the entrainment of irrotational fluid in large amounts; figures 7(*b*), 8(*b*), and 9(*c*) clearly show the potential-flow wedge between two adjacent large structures. This indicates that the flow is highly intermittent, a characteristic which also has been evident in the early pictures of Ramsey & Goldstein (1971).

As a result of all the observations mentioned above, an idealized flow model for the laminar-flow case has been sketched in figure 10. It is an *instantaneous* picture of the flow, as opposed to the mean-flow picture presented by Andreopoulos & Rodi (1984) and Foss (1980), and it shows the rolling up of the annular laminar boundary/shear layer, which has an initial vorticity as well as additional vorticity generated at the interface by its strong shear with the cross-stream. Very close to the exit, these vortex rings are significantly stretched because their parts at the lee side of the jet are highly accelerated for a downstream distance of a few diameters. During that time the strongly stretched legs of successive vortical rings can bundle up to form the so-called bound vortex, and a breakdown to turbulence can take place. However, these vortical rings can be considered as open at their lower side because of the compression of their vortex lines by the negative lateral gradient $\partial W/\partial z$. Further downstream the relative movement between the upper and lower jet fluid

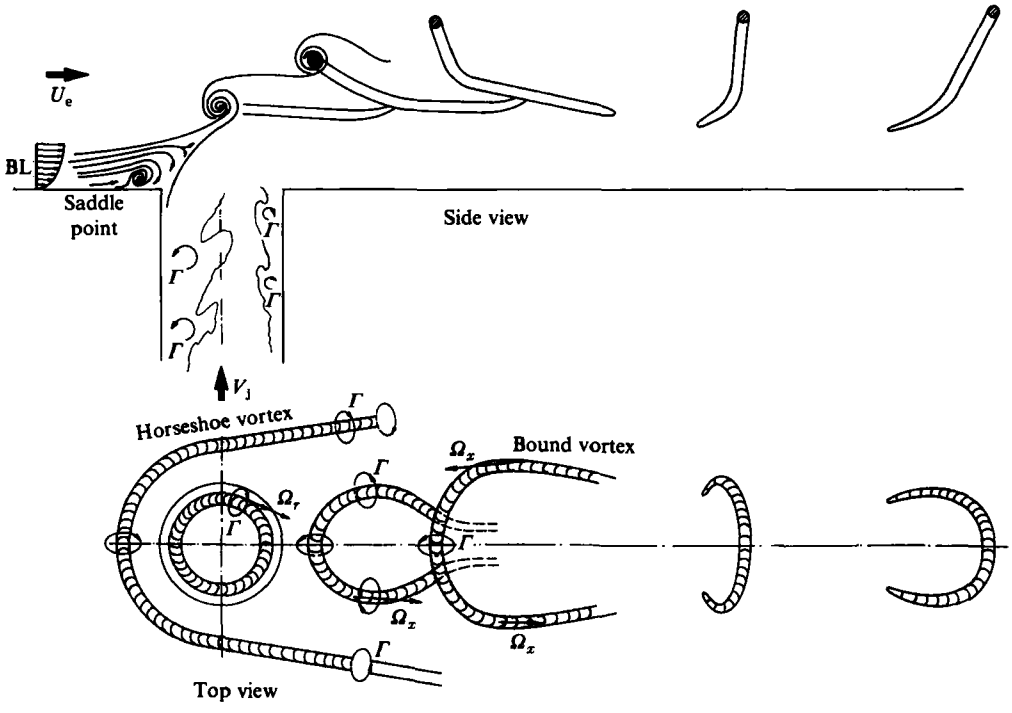

FIGURE 10. Proposed vorticity pattern and flow configuration.

becomes smaller and smaller, and the vorticity diffuses significantly. At some distance, the outer flow moves faster than the inner flow and structures with opposite vorticity appear. This change of the vorticity content of the large structures seems to be a characteristic feature of the flow, and it is probably caused by the wake which is formed in the lee side of the jet and/or by the wall, i.e. by applying a strong positive mean-velocity gradient $\partial U/\partial y$.

Vortex structures of the above type were observed in chimney smoke a long time ago (see Scorer 1958). Perry & Lim (1978) and Perry & Tan (1984) have reproduced and controlled similar vortex loops formed by a laterally oscillating axisymmetric jet in a co-flowing uniform stream. In the present situation the basic structure emanating from the pipe exit seems to show some similarities to the vortex loops of Perry & Lim, and Perry & Tan, but it seems that the presence of the *crossflow* and the *wall* differentiate strongly the two flows. From the above discussion it is clear that these two characteristics affect dramatically the vortex dynamics of the present flow and therefore they are two additional parameters which complicate the phenomenon.

The above oversimplified flow model can also be applied to turbulent flow if, in the above discussion, the vortex rings were replaced by vorticity-containing eddies. In the turbulent-flow case, particularly at medium or higher Reynolds numbers, the appearance of such vortical structures is not regular. In addition, as these structures are coming out of the pipe, they interact with the oncoming flat-plate boundary-layer eddies which carry *opposite* vorticity. It might then be expected that between two pipe eddies, a boundary-layer eddy could be also transported by the flow and interact with the former. Thus flat-plate boundary-layer eddies, with opposite vorticity to

that of the pipe eddies, may significantly help the vorticity diffusion of the latter eddies in the immediate downstream region.

Entrainment of potential core fluid of the pipe flow by the large structures outside the pipe may also be significant. The role of these structures in the entrainment of irrotational fluid is not clear from the flow visualization since the smoke tags the whole pipe flow. The conditionally sampled results presented below can give some more information on the role of the irrotational fluid in general, and on the interaction of the boundary-layer eddies with those of the pipe in particular.

3.3. *Conditional-sampling analysis*

Conditionally sampled results have been obtained at one velocity ratio $R = 0.5$ and one Reynolds number $Re = V_j D/\nu = 20500$. Under these conditions the large-scale structures have an irregular character, without any regular shedding of vorticity from the mouth of the jet. Measurements have been taken at seven downstream positions at the plane of symmetry ($z/D = 0$), $x/D = -0.25$, 0, 0.25, 0.5, 2, 4, and 6. The first four positions are stations above the exit, in the immediate region of the interaction, while the remaining three positions represent stations in the downstream region.

3.3.1. *Intermittency profiles*

Figures 11 (*a*)–(*g*) show the intermittency profiles for the four postulated flow zones at various downstream positions. Since any fluid particle must belong to one of the four mutually exclusive zones, that is CN, CT, HN and HT, the addition law of (1) reduces to

$$\gamma_{HT}+\gamma_{HN}+\gamma_{CT}+\gamma_{CN} = 1.$$

The profiles at $x/D = -0.25$ in figure 11 (*a*) clearly show that cold, turbulent fluid (CT) has penetrated the hot jet flow down to the exit plane $y/D = 0$. In other words, there is a significant ($\simeq 3\%$) probability of finding boundary-layer turbulent fluid on the exit plane, where the probability of finding turbulent pipe fluid (HT) is about 36.5%. However, as expected, there is more of the irrotational pipe fluid (HN) here, while the cross-stream irrotational fluid (CN) has an extremely low probability of appearance. At higher y/D distances above the exit, the intermittency factors of both HN and CN fluids vary monotonically with y/D: that of HN is reduced and practically vanishes at $y/D \geqslant 0.25$ while that of CN increases (particularly above $y/D = 0.25$) and must, as shown by (1), reach a value of 1 at some further y distances. The behaviour of the pipe- and boundary-layer-turbulent-fluid intermittency factors is quite different; the probability of finding HT fluid increases with y/D and at $y/D = 0.15$ reaches its highest value of 73.5%. Then, it reduces rapidly and at the last measuring point where $y/D = 0.4$ has a value of only 5%. The probability of finding flat-plate boundary-layer fluid increases with y/D, with a maximum at about $0.30D$ away from the exit.

The behaviour of the intermittency profiles at the next downstream station (figure 11*b*) is generally similar, although some strong quantitative differences exist. At smaller positions than $y/D = 0.25$, the probability of finding cross-stream fluid, rotational or irrotational, is extremely low, i.e. the flow there has a 'time sharing' character between the turbulent and non-turbulent pipe flow. In addition, the maxima of the γ_{HT}- and γ_{CT}-distributions take place at greater y/D than at $x/D = -0.25$. This means that at further downstream stations the interaction begins

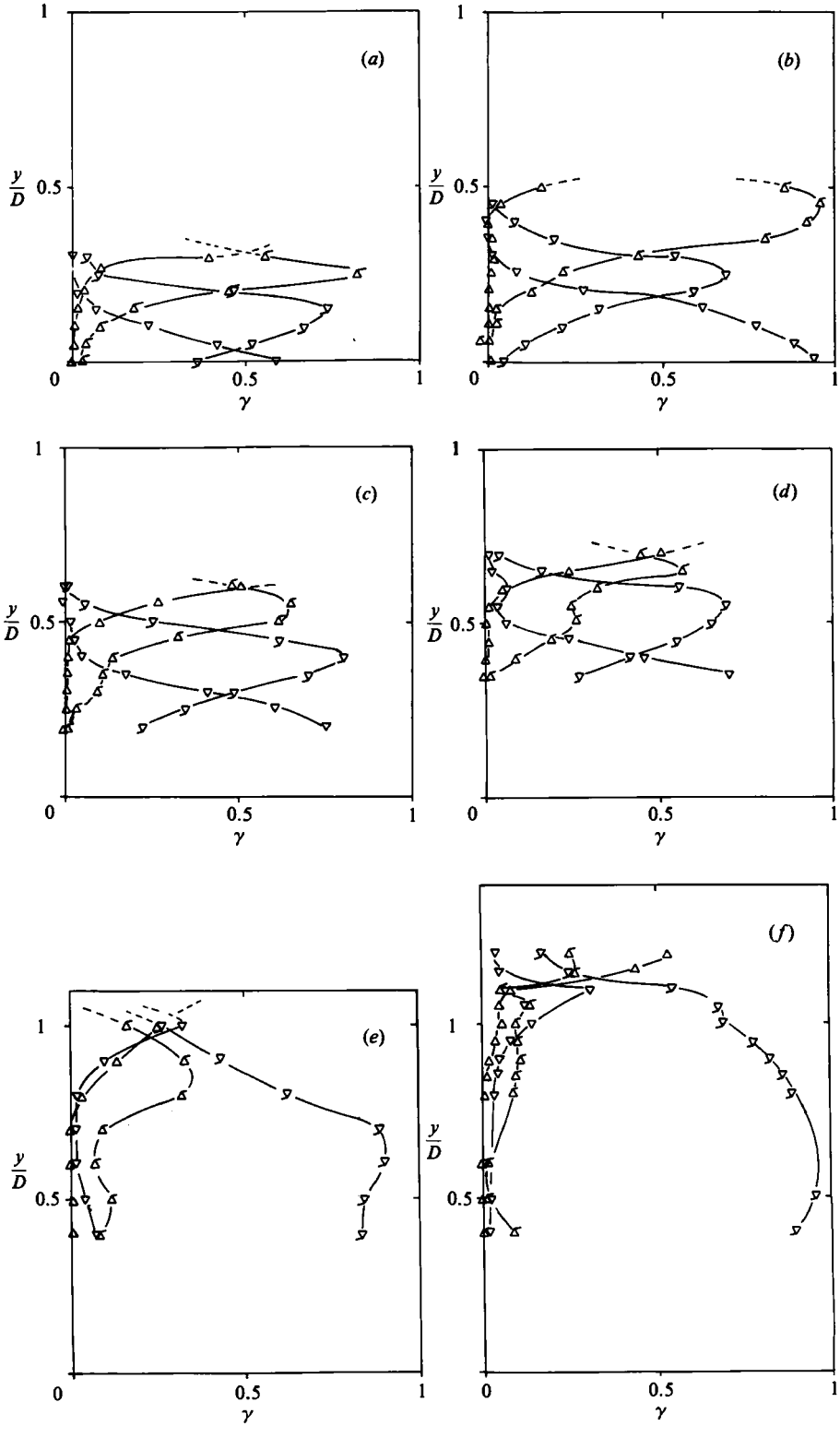

FIGURE 11 (*a–f*). For caption see opposite page.

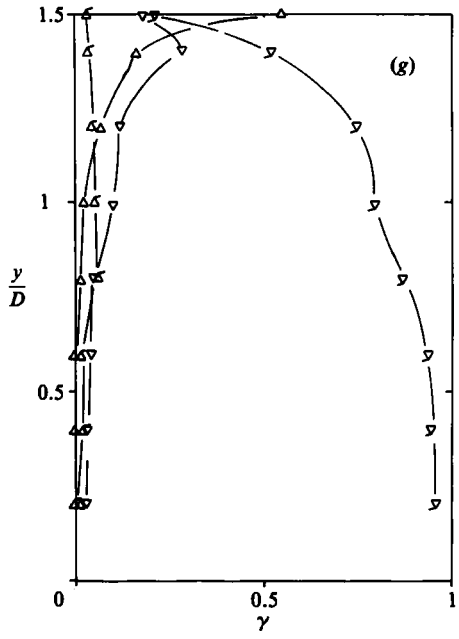

FIGURE 11. Intermittency profiles: (*a*) $x/D = -0.25$; (*b*) 0, (*c*) $+0.25$; (*d*) 0.5; (*e*) 2; (*f*) 4; (*g*) 6. ∇, HN; $\triangledown$, HT; $\triangle$, CH; $\blacktriangle$, CT. Mnemonic: rising plume for Hot zone values, iceberg for Cold zone values, flagged symbols for Turbulent zone values, non-flagged symbols for Non-turbulent zone values.

at higher distances from the exit. The profiles at the next station $x/D = +0.25$ (figure 11*c*) exhibit the same behaviour in that respect.

All the intermittency profiles at positions above the exit show that there are quite large regions of the flow which received significant contributions from all of the four possible zones. There are, of course, regions where the flow 'time shares' partially, between two or three of the four postulated zones.

The profiles of γ at the next downstream stations (figure 11*d*) exhibit different boundary-layer-eddy behaviour, as shown by the small plateau of γ_{CT} at $y \simeq 0.5$. The profiles of γ_{CT} at the upstream stations show that these cold eddies travel downstream, passing over the exit, and are probably lifted by the jet flow. At $x/D = 0.5$, however, eddies can also arrive by travelling *around* the exit, entering the reverse-flow region behind the jet exit before being lifted up.

The probability of finding turbulent boundary-layer fluid at $x/D = 2$ and 4 drops drastically, as is seen in figures 11 (*e*) and (*f*), but even at $x/D = 6$ (figure 11*g*), this probability has values of the order of 5%.

It is also interesting to see the increase of the amount of pipe irrotational fluid (HN) at the outer edge of the curved jet. Figure 11 (*f*) shows such an increase of γ_{HN} up to a distance of $y/D \simeq 1.1$ Beyond that position, γ_{HN} reduces very quickly, a behaviour which is not obvious at $x/D = 2$ because no measurements are available to show that decrease at that station.

At the station where $x/D = 6$ the CT fluid becomes rare, i.e. the probability of finding any boundary-layer eddy is less than 6%.

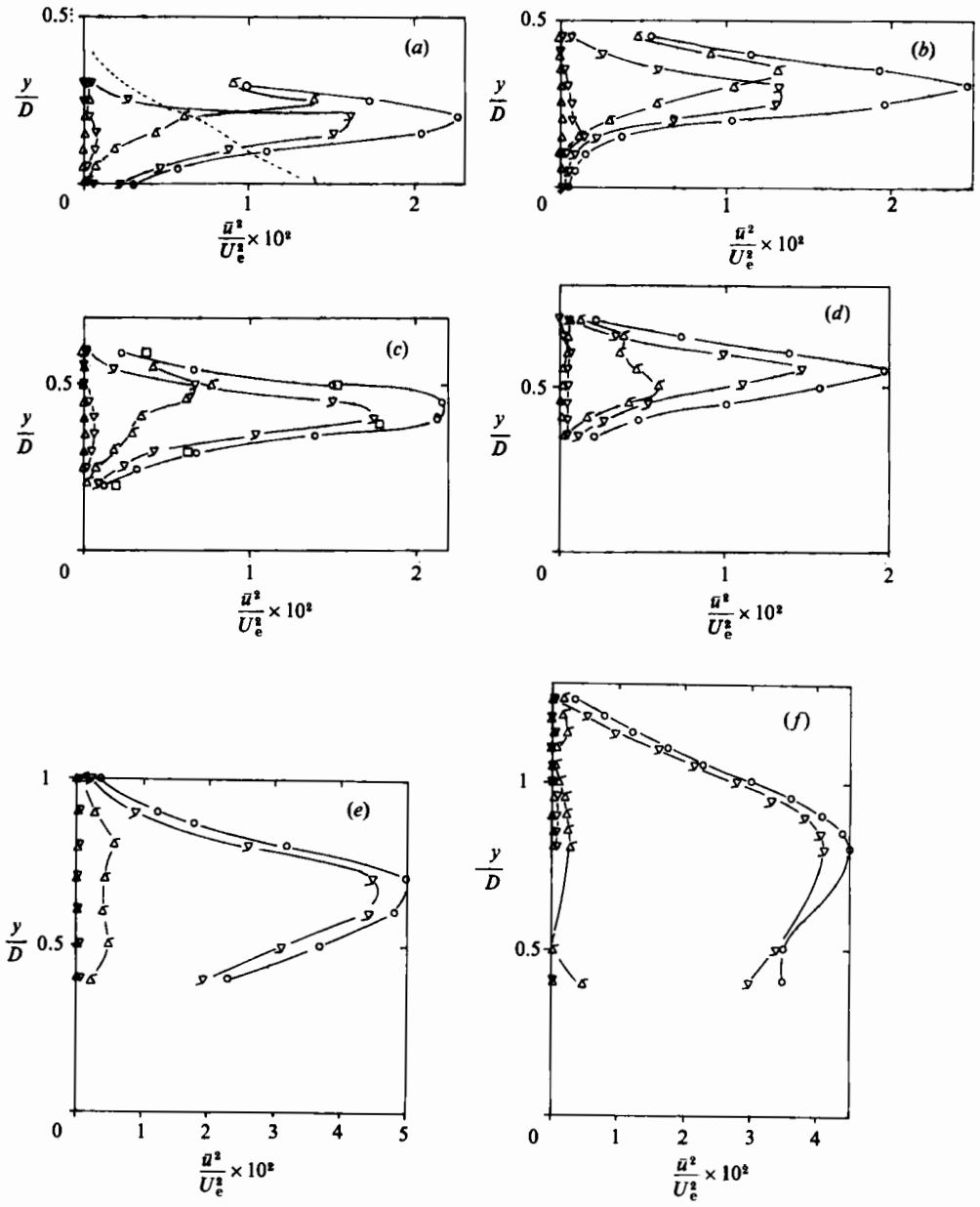

FIGURE 12(*a–f*). For caption see opposite page.

3.3.2. *Reynolds stresses and triple products*

Figures 12–19 show conditional and conventional averages of turbulent quantities. The former are plotted as *contributions* to the latter using (1). Profiles of the normal and shear stresses $\overline{u^2}$, $\overline{v^2}$ and $\overline{uv}$ are shown in figures 12–14 for the seven aforementioned downstream stations at the plane of symmetry $z/D = 0$. It is clearly shown that the two turbulent fields start to interact strongly soon after they meet and that these turbulent fields are the main contributors to the total average quantities; the irrotational fluctuations of the cross-stream have an almost zero contribution, although those of the pipe sometimes contribute significantly. This trend is particularly

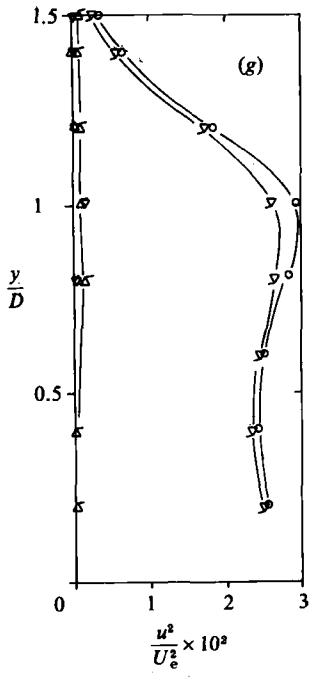

FIGURE 12. u^2-profiles: (*a*) $x/D = -0.25$; (*b*) 0; (*c*) +0.25; (*d*) +0.5; (*e*) 2; (*f*) 4; (*g*) 6. ○, conventional values; -----, profile at $x/D = -0.5$ taken from Andreopoulos & Rodi (1984); □, triple-wire sensor; other symbols as in figure 7.

evident in the $\overline{v^2}$-profiles at stations over the exit plane (figures 13*a*, *b*, *c* and *d*). There, hot-fluid irrotational fluctuations can account for 25–30% of the conventional $\overline{v^2}$-average and this is 2–3 times greater than their contributions to the $\overline{u^2}$-conventional average.

The fact that the irrotational fluctuations are appreciable only for $x/D < 0.5$ gives some more evidence for the shedding of large structures which cause the expected irrotational effects like $\overline{v^2_{\mathrm{HN}}} \gg \overline{u^2_{\mathrm{HN}}}$ in all potential regions outside the shear layers.

The measurements of $\overline{uv}$ are shown in figure 14. The shear stress correlation coefficient $R_{uv} = \overline{uv}/\sqrt{\overline{u^2}}\sqrt{\overline{v^2}}$ reflects the behaviour of $\overline{uv}$ and it is therefore not shown here. The conventional $\overline{uv}$ data shown in figure 14(*a*) change sign at small y/D. According to Andreopoulos (1982) and Andreopoulos & Rodi (1984) this change of sign is owing to the streamline curvature and deceleration of the flow. In this region the CT-fluid contributions are small and $\overline{uv}$ has positive values, indicating that streamline curvature and deceleration of the *pipe flow* are responsible for the change of sign of the conventional values of $\overline{uv}$.

In figures 12(*a*), 13(*a*) and 14(*a*) the profiles of $\overline{u^2}$, $\overline{v^2}$ and $\overline{uv}$ at $x/D = -0.50$ are also plotted for direct comparison. These profiles correspond to those measured by Andreopoulos & Rodi and are now shown as a broken line. Mixing between 'hot' and 'cold' fluid, for this particular case of $R = 0.5$, has not yet started at $x/D = -0.50$, except in the region very close to the wall ($y/D < 0.05$) where some 'hot' fluid can be found but with very low intermittency. Therefore, it can be concluded that the measurements of Andreopoulos & Rodi closely represent conditional averages of quantities of boundary-layer fluid, i.e. these quantities at $x/D = -0.5$ can be directly compared with the downstream profiles of conditional averages of 'cold and turbulent' fluid. This observation can give us an indication of the strength of the

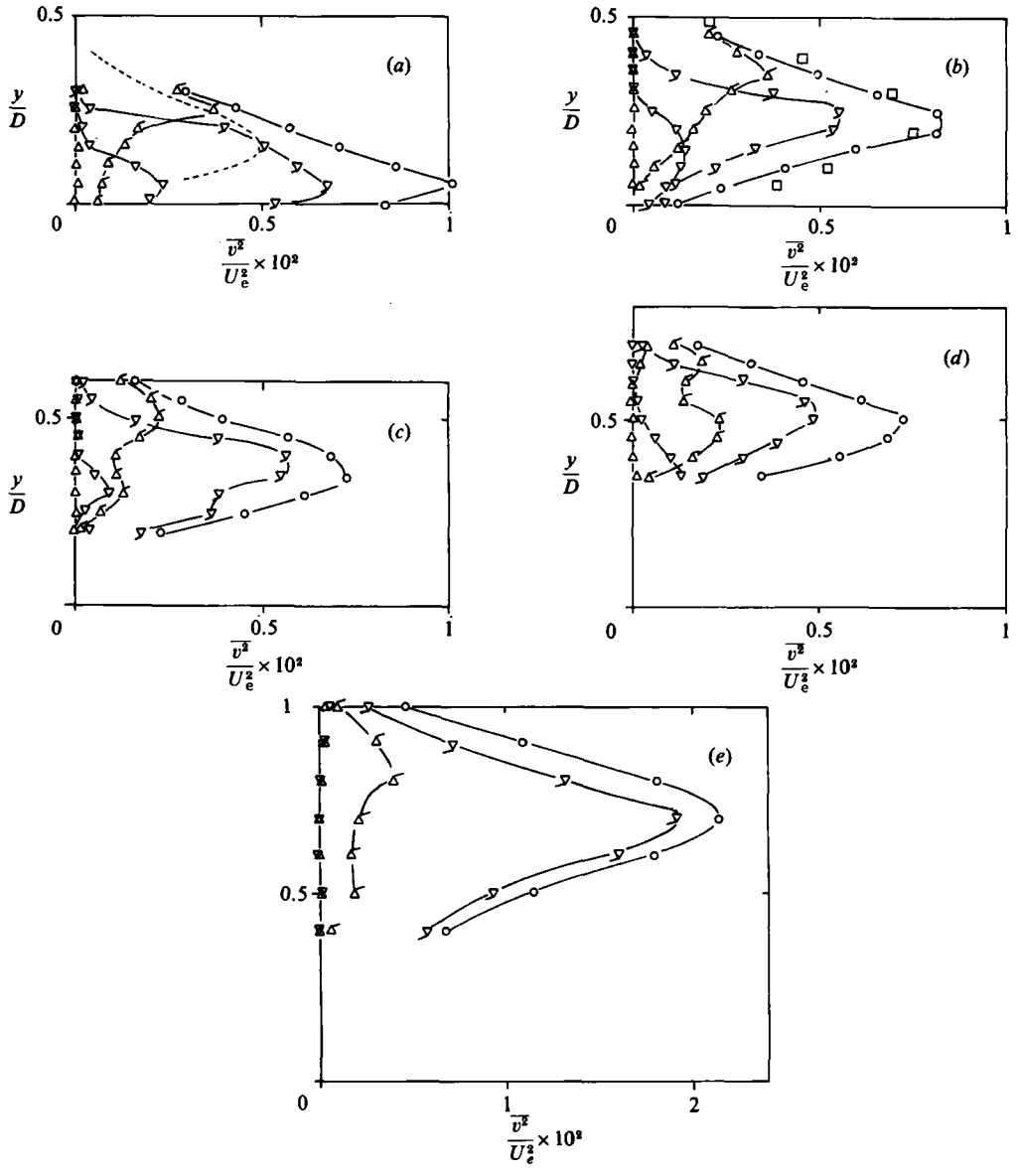

FIGURE 13(*a–e*). For caption see opposite page.

interaction in the near-field region. For example the downstream profiles of CT fluid have decreased dramatically from those upstream. This behaviour is typified in figure 15 where the maximum values of the 'cold and turbulent' zone of each downstream station are plotted against x. Among the three stresses, the normal stress $\overline{u_{CT}^2}$ seems to be drastically affected by the interaction; within less than one diameter from the point where the interaction has started, roughly at the upstream edge of the pipe, it has reduced by more than 50 % of its initial value and it continues to decay slowly further downstream.

The intensity profiles of the boundary-layer turbulent zone at $x/D = 0.5$ form their maximum values at the lower side of the conventional profile, i.e. closer to the side with positive gradient $\partial\overline{u^2}/\partial y$. In contrast, the profiles upstream show their maxima

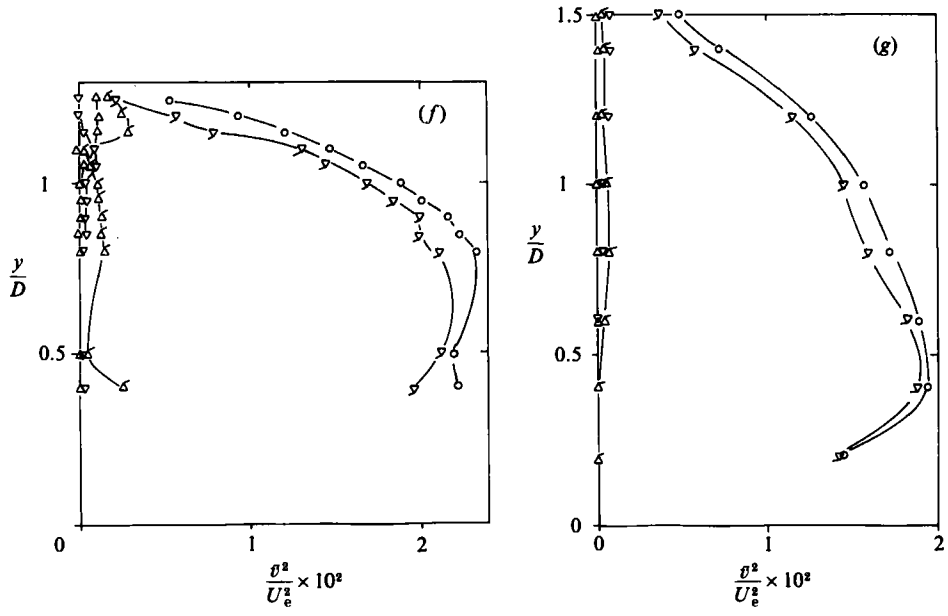

FIGURE 13. $\overline{v^2}$-profiles: x/D values and symbols as in figure 8.

towards the side with the negative gradient. As in the case of the intermittency distribution of γ_{CT} at $x/D = 0.5$, the above feature can also be attributed to the arrival of eddies which travelled around the exit and were then lifted up. In addition to the mean advection, turbulent transport of the stresses by the triple products from upstream also takes place.

The reader is reminded that the values at $x/D = -0.50$, which serve to indicate the distortion of the downstream profiles by the interaction, are not typical boundary-layer data and therefore not to be directly compared even with data from a strongly decelerated boundary layer. It is also clear from the profiles of the normal and shear stresses that at stations downstream of the pipe exit, contributions from the boundary-layer turbulence (CT fluid) become smaller, as opposed to those from the HT fluid which increase and asymptotically tend to the conventional averages.

Figures 16–19 show the triple velocity products; large differences can be discerned between the contributions from the four different zones for the conventional quantities, including changes in sign. Again, contributions by the irrotational fluid here are relatively small, particularly those contributed by the free stream of the crossflow. Contributions by the pipe irrotational flow, however, are more evident in the profiles of $\overline{v^3}$, $\overline{u^2v}$ and $\overline{uv^2}$ over the exit, and mainly at low y/D distances. The reason why only quantities including v are most affected by these irrotational fluctuations can be attributed to effects associated with the shedding of large structures.

3.3.3. *Zone-averaged velocities*

The total picture of the flow would be incomplete without showing the zone-averaged velocity $\tilde{U}$ and $\tilde{V}$ profiles and they are given in figures 20 and 21. Note that the addition law (1) does *not* hold for these quantities. Instead of plotting $\tilde{U}$ and $\tilde{V}$ separately at various downstream stations, it was felt that a vector presentation of these quantities would be more informative. The vectors are plotted relative to the

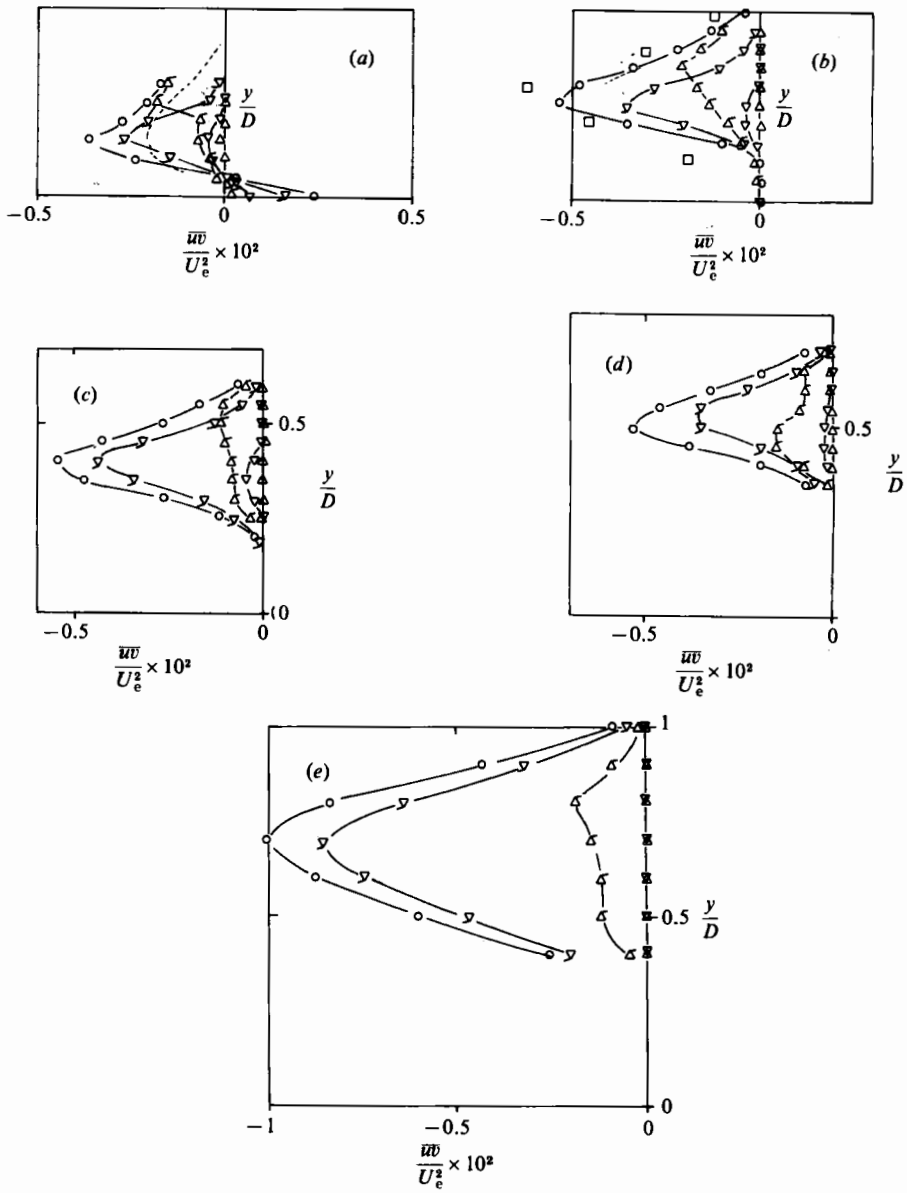

FIGURE 14(*a–e*). For caption see opposite page.

mean velocity vector, that is, their components are $\tilde{U} - \overline{U}$ and $\tilde{V} - \overline{V}$. Figure 20 shows profiles of zone-averaged velocity vectors at various downstream stations for the pipe flow. Similar profiles for the boundary-layer flow are plotted in figure 21. Iso-intermittency contours for each of the four zones and for two values of γ are also plotted on these figures for visual aid. In particular the contours for $\gamma = 0.01$ give a good indication of the zone edges.

Both figures show large differences between zonal-averaged velocity vectors and the conventional mean-velocity vectors almost everywhere in the flow except probably in the outer part of the curved jet. These differences can reach values greater than 15% of the free-stream velocity U_e. The fact that differences are smallest near the outer edge of the jet, where the intermittency is small, suggests that the

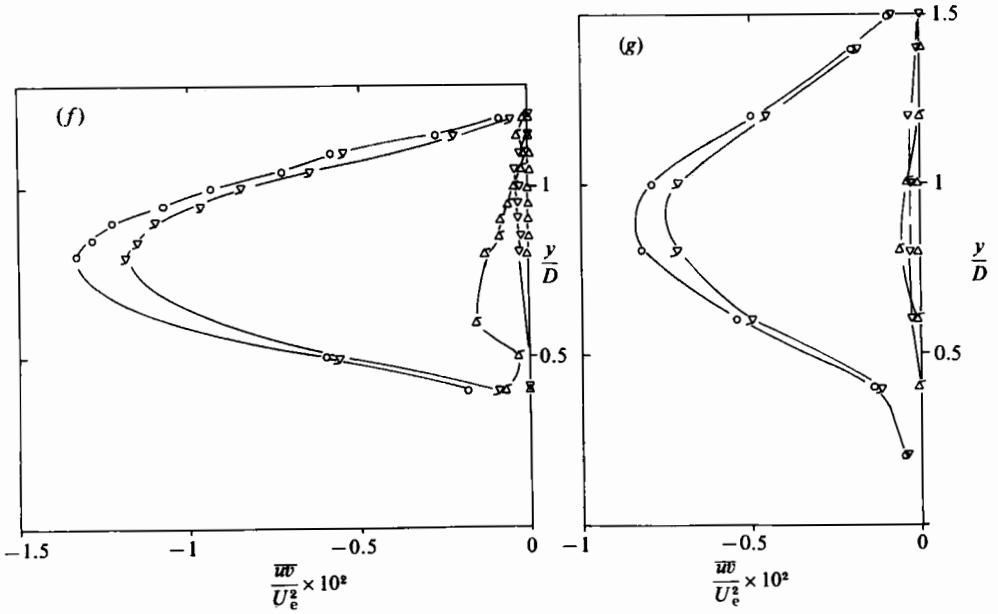

FIGURE 14. $\overline{uv}$-profiles: x/D values and symbols as in figure 8.

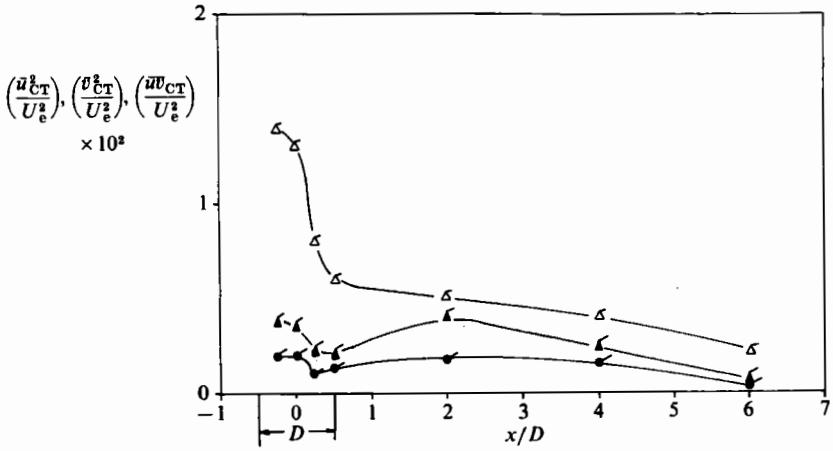

FIGURE 15. Longitudinal decay of maximum stresses of the boundary-layer fluid (CT zone): △, u^2_{CT}; ▲ uv_{CT}; ●, v^2_{CT}.

discrimination technique behaves fairly well; even small errors in the region where $\gamma < 0.2$ would greatly increase the differences between zone-average velocity vectors and conventional mean-velocity vectors.

The vector plots of the HN-fluid are closely related to the entrainment velocity, and their behaviour, shown in figure 20, seems to be rather complicated. Generally, an irrotational-fluid element entrained by sheared fluid retains its zero vorticity until it gains vorticity by the direct action of viscosity. Thus, a study of the flow pattern of the irrotational fluid and that of the turbulent fluid can provide useful information on the first and the last stages of the whole entrainment process. In the region above the exit the inclination of the HN-fluid vector changes very quickly; at the exit, it

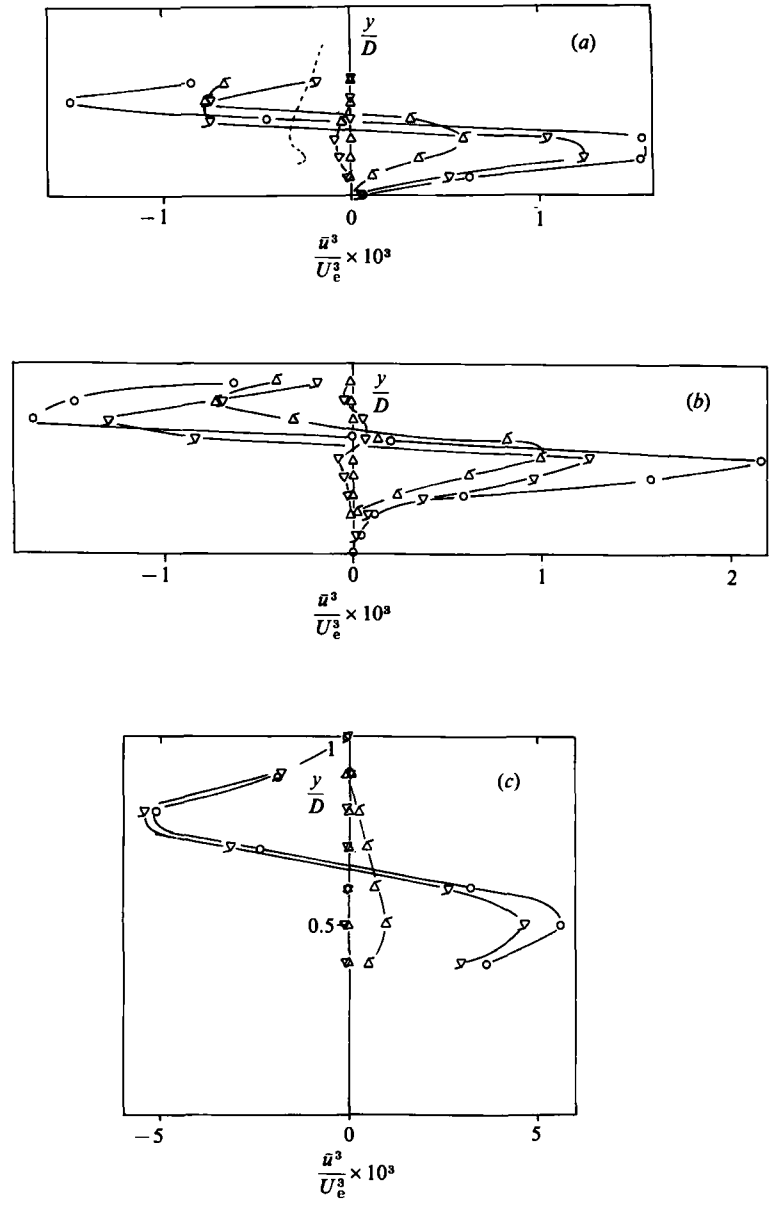

FIGURE 16. $\overline{u^3}$-profiles: (*a*) $x/D = -0.25$; (*b*) 0; (*c*) $x/D = 2$. Symbols as in figure 8.

has an inclination of roughly 90° with respect to the x-axis while at greater y/D it is inclined towards the upstream side of the pipe. At $x/D = 2$ the situation is quite different. In the outer part of the flow the vectors have a negative inclination, i.e. they have a direction towards the wall, while at distances closer to the wall they change direction completely, i.e. they are inclined towards the upstream direction. This region is closely related to the wake region formed behind the jet and it vanishes at further downstream stations (see figure 16). At $x/D = 6$, the velocity vectors of the HN-fluid are inclined towards the wall for almost any distance from the wall.

The behaviour of the HT-fluid vector is also interesting. These vectors are inclined with roughly 0° or 180° angles relative to those of the HN-fluid. It is not clear from

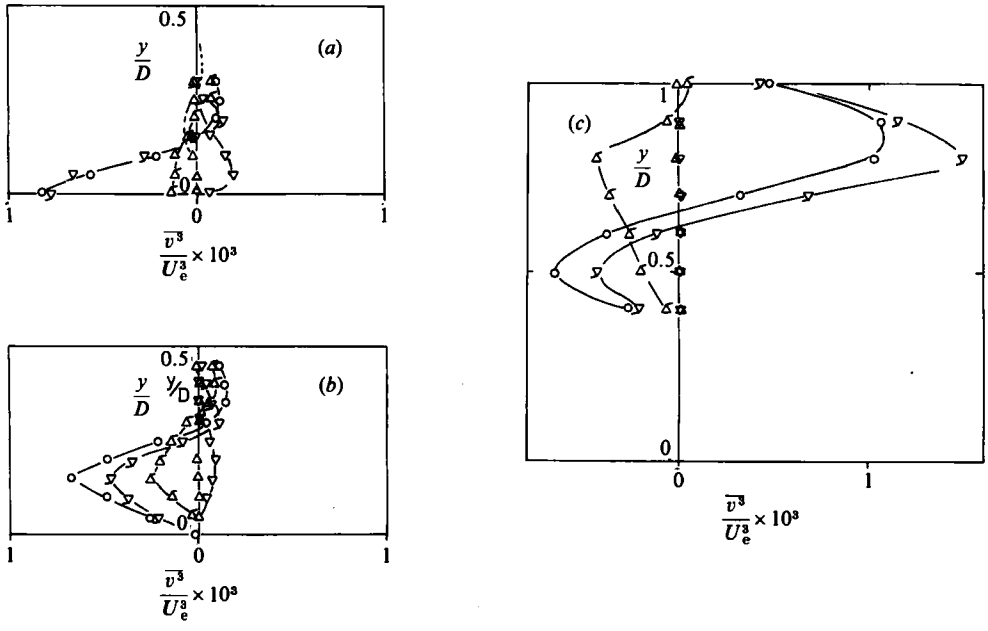

FIGURE 17. $\overline{v^3}$-profiles. x/D values as in figure 19, symbols as in figure 8.

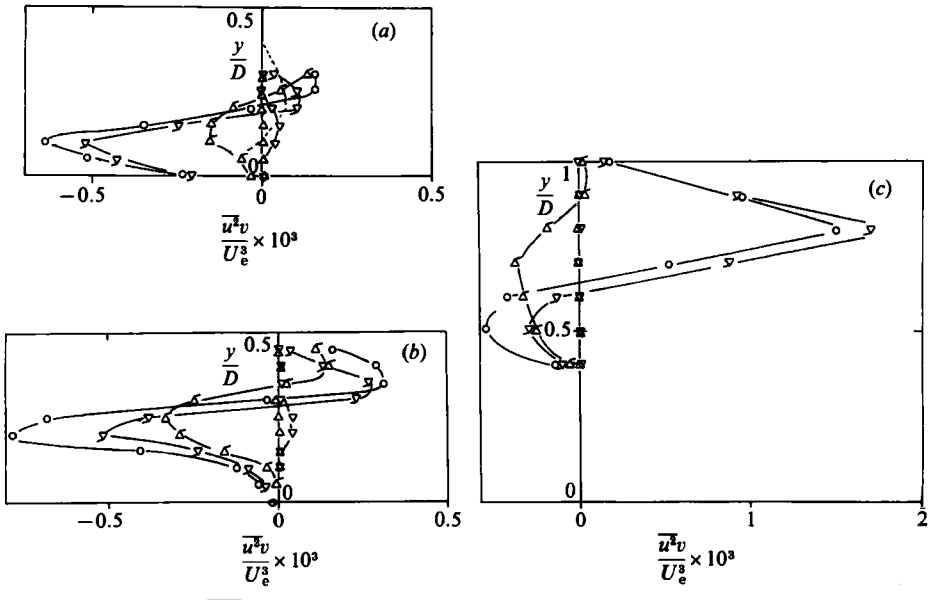

FIGURE 18. $\overline{u^2v}$-profiles. x/D values as in figure 19, symbols as in figure 8.

the present experimental results which of the two relative positions favours more transition to vortical fluid. It can also be seen in figures 22 (*a*) and (*b*) that in simpler turbulent flows, like the jet issuing in still air (Chevray & Tutu 1978) or the boundary layer (Murlis *et al.* 1982), the relative inclination between the HT-fluid vectors and those of the HN-fluid is 180°. Although an extrapolation of this characteristic to the present complex-flow situation seems to be unjustified, it can be argued that the case where the gradient of the vector difference between the velocities of the two fluids

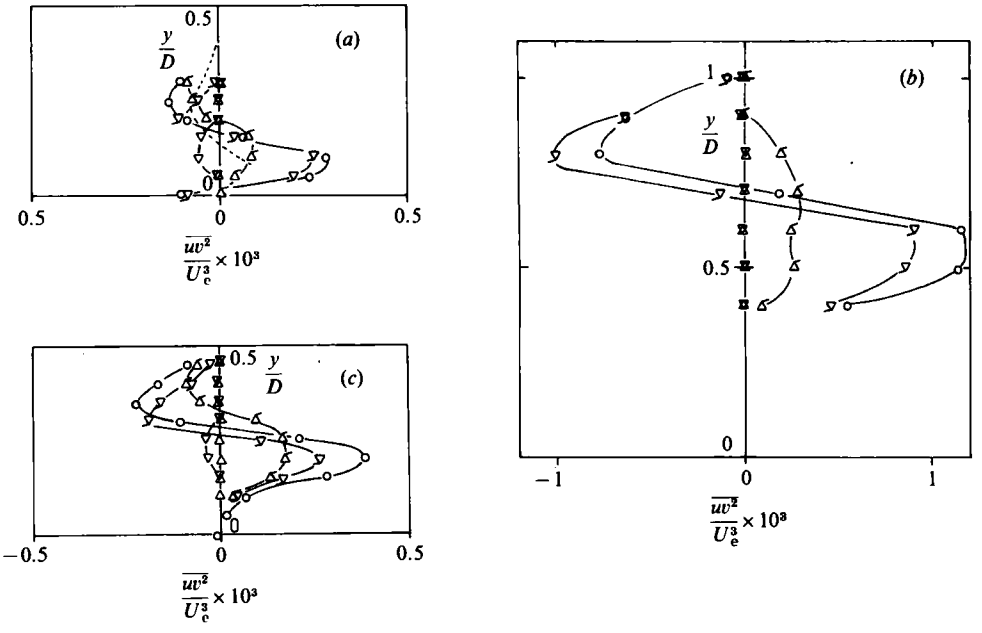

FIGURE 19. $\overline{uv^2}$-profiles. x/D values as in figure 12, symbols as in figure 8.

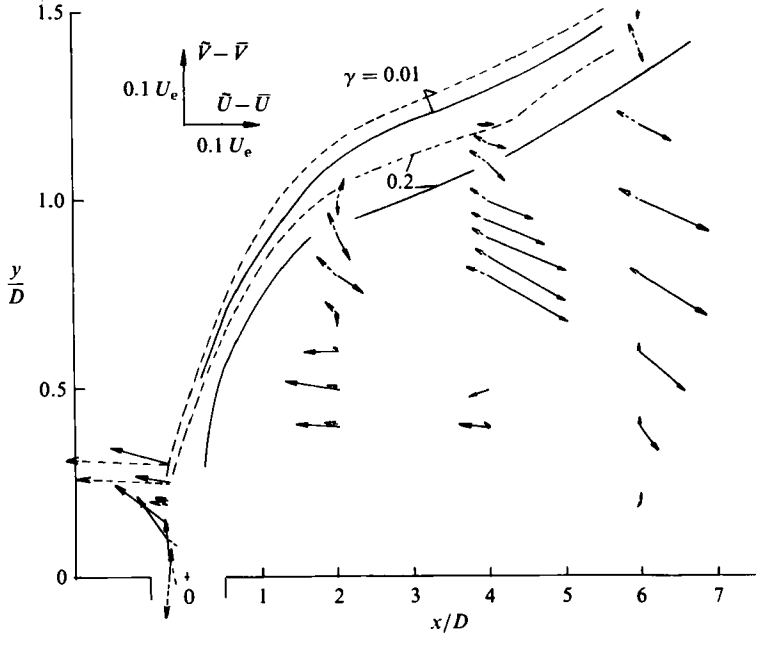

FIGURE 20. Zone-averaged-velocity-vector plot on the plane of symmetry: ——, pipe irrotational fluid (HN); ---- pipe rotational fluid (HT).

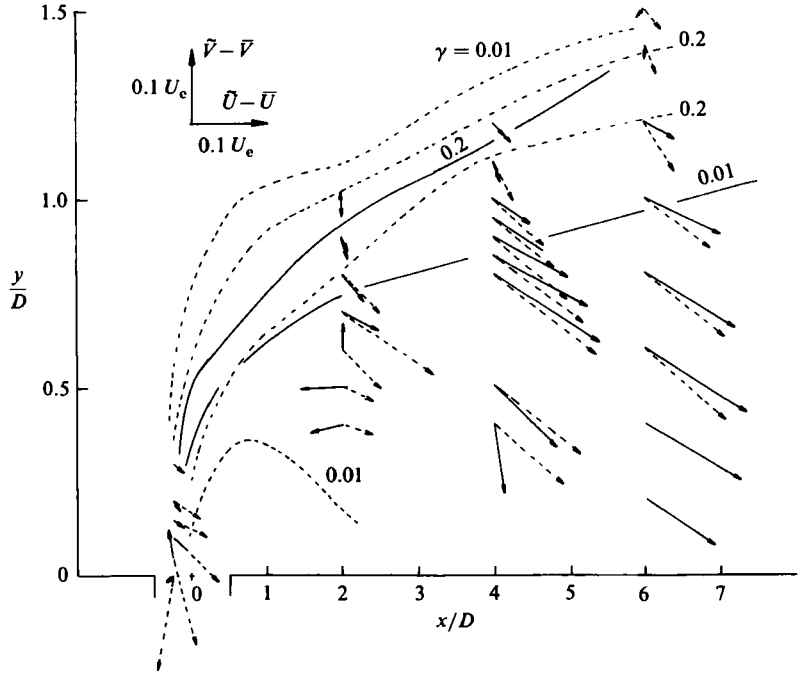

FIGURE 21. Zone-averaged-velocity-vector plots on the plane of symmetry: ——, cross-stream irrotational fluid (CN); --- cross-stream turbulent fluid (CT).

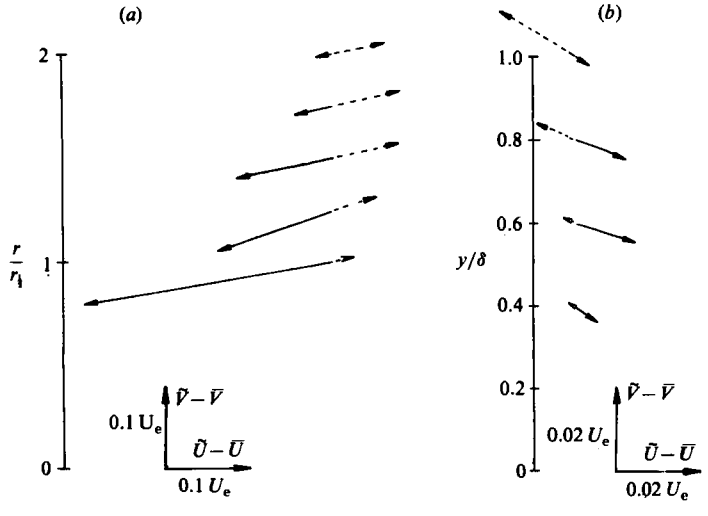

FIGURE 22. (*a*) Zone-averaged-velocity-vector plots of a circular jet issuing in still air, as deduced from the data of Chevray & Tutu (1978): ——, irrotational fluid; ----, rotational fluid. (*b*) Zone-averaged velocity-vector plots of a boundary layer as deduced from the data of Bradshaw, Tsai & Murlis (1982): ——, irrotational fluid; ----, rotational fluid. Note that the velocity scale here is five times smaller than in (*a*).

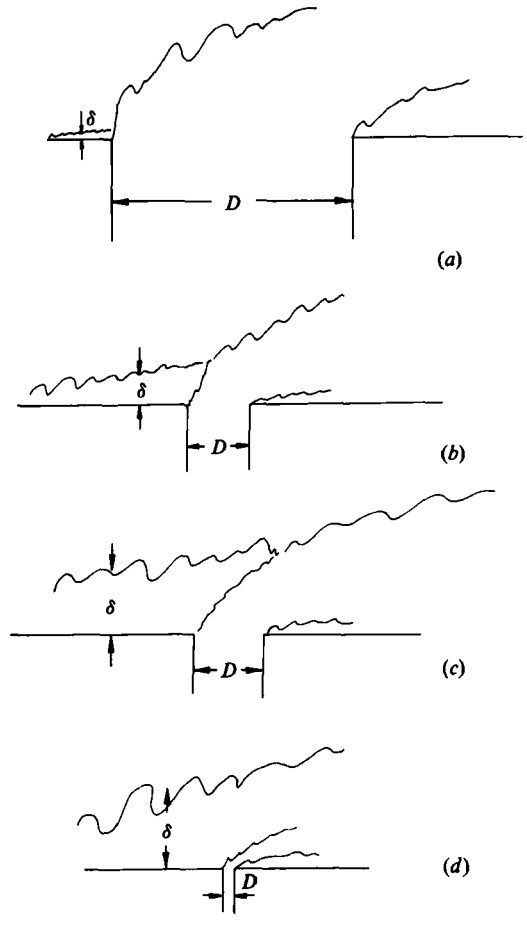

FIGURE 23. Flow configuration as function of δ and D. (*a*) $D \gg \delta$; (*b*) $D > \delta$; (*c*) $\delta > D$; (*d*) $\delta \gg D$.

is high indicates a quicker gain of vorticity by the irrotational fluid. Thus, this might be the case with the 180° angle of relative inclination.

Similar vectors of the CT- and CN-fluid have been plotted in figure 21. In the near field above the exit, the CN-fluid vectors are very small in magnitude but roughly opposite in direction from those of the HN-fluid. The CT-fluid vectors at the exit plane are very large in magnitude and have a direction towards the plenum chamber of the jet. In all other places these CT-fluid vectors have a direction roughly opposite to that of the HT-fluid vectors. It is interesting to see that the relative motion in the far-downstream profiles between the rotational and irrotational fluid coming from the boundary layer is rather small, and much smaller than the relative motion between the irrotational and rotational fluid of the pipe. This is an indication that HN-fluid becomes vortical quicker than the CN-fluid. More generally, it can be argued that the HT-fluid favours transition to vortical flow more than CT-fluid does. This can be justified by looking at all possible relative velocity vectors formed among the four zones. The relative velocity vector formed between the HT-fluid velocity vector and the velocity vector of any of the other two irrotational zones can be five times larger than the relative velocity vector between CT-fluid and any of the other irrotational zones. This simply means that if irrotational fluid originating from the

pipe or the cross-stream is 'surrounded' by HT-fluid, it is more prone to transition than in the situation of being surrounded by CT-fluid simply because the Reynolds number is up to five times-higher in the former case.

4. Conclusions and further discussion

The present experimental investigation reveals the existence of large-scale structures in the flow of a jet in a crossflow. These structures are sometimes well organized and sometimes not, depending basically on the Reynolds number and the velocity ratio $R = V_j/U_e$. At high velocity ratios, say $R > 3$, and low Reynolds numbers, say $Re = V_j D/\nu < 5 \times 10^3$, the annular mixing layer of the pipe rolls up and toroidal vortices are formed, similar to those of a jet issuing into 'still' air, but with different development. These vortices, or vortical rings, or large structures, carry vorticity of the same sign as the flow inside the pipe but opposite to that of the cross-stream turbulent flow, and they are well organized. They are subjected to tilting and stretching, and they break down to turbulence within the first couple of pipe diameters downstream of the exit. As the velocity ratio R decreases the organization of these large structures reduces, but still there is a periodicity in their appearance. The jet mouth sheds large structures with a frequency which, if it is scaled with the cross free-stream velocity U_e and the pipe diameter D, seems to be independent of the velocity ratio and the Reynolds number. These structures grow by pairing and at some distance downstream change their vorticity content. Thus the originally 'jet-like' structure becomes 'wake-like' within a few diameters downstream of the exit. As the Reynolds number increases, say $Re > 5 \times 10^3$, the regularity of the appearance of the large structures leaving the pipe decreases, and the eddies now occupy a wide range of sizes. They interact with upstream boundary-layer eddies of opposite vorticity, grow in size and entrain irrotational fluid. At the end of the interaction region the 'average' eddy shape is similar to that of a 'boundary-layer-like' or 'wakelike' eddy as far as the vorticity content is concerned. In that respect, the vorticity content of the 'average'-eddy, high-Reynolds-number case thus exhibits the same feature as the low-Reynolds-number case. Thus the average vorticity content of the jet in a crossflow far downstream of the jet exit seems to be qualitatively independent of Reynolds number for velocity ratios $R < 2$.

The interaction region for a Reynolds number of 20500 and velocity ratio of 0.5 was explored by means of conditional-sampling techniques using two conditioning functions simultaneously. This was made possible by heating the pipe flow, which allowed for a 'hot'/'cold' discrimination, and then further discriminating the turbulent/non-turbulent interface. The results show that the flow 'time shares' between four possible zones, namely: irrotational cross-stream flow, irrotational pipe flow, turbulent boundary-layer flow which develops over the flat plate, and turbulent pipe flow. The 'time-sharing' concept first introduced by Bradshaw (1975) in the work of Dean & Bradshaw (1976) is used here to describe a flow situation where changes in the turbulent structure of the eddies can take place, while in the original suggestion of Bradshaw it was implied that the eddies time share without changes in their structure.

In the particular case of $R = 0.5$, the conditionally sampled average quantities show that most of the interaction takes place in the region above the exit where the contributions of the cross-stream are very high. This means that the interface between the pipe flow and the boundary layer is quite irregular, and the concept that the crossflow acts like a partial cover over the exit may be quite misleading, even

for the mean-flow picture. However, this concept, which was first introduced by Foss (1980), seems to be valid for laminar flows at Reynolds numbers and low velocity ratios and probably for quite thin flat-plate boundary layers.

The present conditional-sampling analysis has also shown that a large percentage of the measured normal stresses, in the region near the exit, is due to free-stream irrotational fluctuation. Thus, fluctuations of 'genuine' turbulence are always overestimated in the vicinity of the jet exit. Generally, the interaction between the jet and the boundary layer is quite strong and among the three stresses the $\overline{u^2_{CT}}$ seems to be drastically affected. It was also found that, in the downstream region, the irrotational fluid, regardless of its origin, moves faster than the mean flow and that the turbulent-pipe-flow fluid is always slower than any of the other three types of fluids. This is probably an indication that this relative motion between turbulent pipe flow and any of the two irrotational flows favours transition to turbulence of the irrotational fluid more than any other relative motion.

At stations farther downstream the jet turbulent-fluid contributions to all turbulent quantities closely approach the conventional averages, while the boundary-layer turbulent-fluid contributions tend to zero. The distance where this takes place is difficult to estimate for the general case and needs further investigation. It seems plausible, however, that this distance depends on the relative size of the lengthscales of the initial flows (for a given velocity ratio R). This is, in fact, justified by using some *crude* order-of-magnitude analysis: at the point where the HT-fluid contributions approach the conventional averages and CT-fluid contributions tend to zero,

$$\mathscr{U}_{HT} \gg \mathscr{U}_{CT} \tag{2}$$

where $\mathscr{U}$ is a turbulent-velocity scale which is proportional to a typical length-scale of the energy-containing eddies, which again is a fraction of the thickness of the shear flows. Then, (2) is equivalent to

$$D \gg \delta \tag{3}$$

where δ is the boundary-layer thickness. Thus, in the flow situation shown schematically in figure 23(*a*) the boundary-layer turbulent fluid is expected to diffuse very quickly inside the larger-scale turbulence of the jet. Consequently, the distance where the jet turbulent-fluid contributions approach the conventional averages is rather short. If δ is of the order of magnitude of D (see figure 23*b* and *c*) then this distance seems to increase with increasing ratio δ/D. This tendency is not, however, maintained for very large values of δ/D. If $\delta \gg D$ (figure 23*d*) then the turbulence of the pipe flow diffuses very quickly. In this case boundary-layer-fluid contributions approach the conventional total averages and the pipe contributions asymptote to zero. Although the above discussion on the length of the interaction region is rather naïve, because it is based on superposition arguments which assume no interaction, it has shown that further investigation is required for better qualitative or even quantitative description of the interaction. The present investigation has covered the case of $\delta/D \simeq 0.34$ only, i.e. that shown in figure 23(*b*). The other cases shown in figure 23 can be the subject of another investigation in the future.

The research reported in this paper was sponsored by the Deutsche Forschungsgemeinschaft during the author's tenure at the University of Karlsruhe. The author would like to acknowledge useful discussions and comments provided by Professors J. F. Foss, D. H. Wood and A. J. Smits, and the technical assistance of Mr D. Bierwirth.

Appendix. Uncertainties and errors in measurement

The transverse gear on which the probe was mounted was driven by three stepping motors, allowing a positioning of the probe with an accuracy of 0.025 mm in the y- and z-directions and 0.1 mm in the longitudinal direction. Extra production of turbulence due to buoyancy was negligible since the flux Richardson number was of the order of 10^{-5}. Therefore the measurement errors originate from one main source: the limitations on the hot-wire technique. One limitation arises from the fact that the velocity component W has not been taken into account in the hot-wire response equation, on the grounds that U and V are the main velocity components if superposition arguments are applied (see Andreopoulos 1982). This assumption causes some error in the results and this error was estimated by Tutu & Chevray (1975), and more recently by Kawall, Shork & Keffer (1983). A second limitation is due to the inability of the hot-wire to distinguish the direction of the velocity vector and this becomes particularly evident at high turbulence intensity (rectification effect). From Tutu & Chevray's Table II, an error due to combined effects of high turbulence intensity and lack of sensitivity to the W-component is quoted for 30 % turbulence intensity as follows: 6.3 % error on $\overline{U}$, 5.2 % on $\overline{u^2}$, 11.9 % on $\overline{v^2}$ and 13.6 % on $\overline{uv}$. The present measurements are in agreement with the triple-wire data of Andreopoulos & Rodi (1984). Some comparisons are given in figures 12(*c*), 13(*b*) and 14(*b*). The two sets of data are unlikely to agree perfectly because, first, the cross-wire performance is poorer than the triple hot wire in high turbulence intensities (see Andreopoulos 1983*a*), and secondly because the effect of the lateral velocity component W was not taken into account in the expression for the effective velocity of the cooling law for the cross wire but W was taken into account for the triple-wire data of Andreopoulos & Rodi.

REFERENCES

Andreopoulos, J. 1981 Comparison test of various hot wire data analysis methods with respect to their performance at various pitch angles. *Rev. Sci. Instrum.* **52**, 1376.

Andreopoulos, J. 1982 Measurements in a jet-pipe flow issuing perpendicularly into a cross-stream, *Trans. ASME* I: *J. Fluid Engng* **104**, 493–499.

Andreopoulos, J. 1983*a* Statistical errors associated with probe geometry and turbulence intensity in hot wire anemometry. *Physics E: Sci. Instr.* **16**, 1264–1271.

Andreopoulos, J. 1983*b* Heat transfer measurements in a heated jet-pipe flow issuing perpendicularly into a cold stream. *Phys. Fluids* **26**, 3201–3210.

Andreopoulos, J. & Bradshaw, P. 1980 Measurements of interacting turbulent shear layers in the near wake of a flat plate. *J. Fluid. Mech.* **100**, 639–668.

Andreopoulos, J. & Rodi, W. 1984 An experimental investigation of jets in a crossflow. *J. Fluid Mech.* **138**, 93–127.

Antonia, R. A. 1981 Conditional sampling in turbulence measurements. *Ann. Rev. Fluid Mech.* **13**, 131.

Antonia, R. A., Prabhu, A. & Stephenson, S. 1975 Conditionally sampled measurements in a heated turbulent jet. *J. Fluid Mech.* **72**, 455.

Bradbury, K. J. S. & Khadem, A. H. 1975 The distortion of a jet by tabs. *J. Fluid Mech.* **70**, 801–813.

Bradshaw, P. 1975 Mixing in complex turbulent flows. In *Proc. Project Squid Workshop, Purdue University, May 1974*, (ed. S. N. R. Murthy). Plenum.

Bradshaw, P. & Murlis, J. 1974 On the measurement of intermittency in turbulent flows. *Imperial College Aero Rep.* 74–04.

CHEN, C.-H. P. & BLACKWELDER, R. F. 1978 Large-scale motion in a boundary layer: a study using temperature contamination. *J. Fluid Mech.* **89**, 1–31.

CHEVRAY, R. & TUTU, N. K. 1978 Intermittency and preferential transport of heat in a round jet. *J. Fluid Mech.* **88**, 133–160.

CORRSIN, S. & KISTLER, A. L. 1955 Free stream boundaries of turbulent flows. *NACA Rep. No.* 1244.

CROW, S. C. & CHAMPAGNE, X. 1971 Orderly structure in jet turbulence. *J. Fluid Mech.* **48**, 547–591.

DEAN, R. B. & BRADSHAW, P. 1976 Measurements of interacting shear layers in a duct. *J. Fluid Mech.* **78**, 641–676.

FABRIS, G. 1979 Conditional sampling study of the turbulent wake of a cylinder. *J. Fluid Mech.* **94**, 673–709.

FIEDLER, H. & HEAD, M. R. 1966 Intermittency measurements in the turbulent boundary layers. *J. Fluid Mech.* **25**, 719.

FOSS, J. F. 1980 Interaction region phenomena for the jet in a cross-flow problem. *Rep. SFB* 80/E/161, University of Karsruhe.

GOLDSCHMIDT, V. M. & BRADSHAW, P. 1973 Flapping of a plane jet. *Phys. Fluids* **16**, 354.

GUTMARK, E. & WYGNANSKI, I. 1970 The planar turbulent jet. *J. Fluid Mech.* **73**, 465.

HEDLEY, T. B. & KEFFER, J. F. 1974 Turbulent non-turbulent decisions in an intermittent flow. *J. Fluid Mech.* **64**, 675.

JENKINS, P. E. & GOLDSCHMIDT, V. W. 1976 Conditional temperature and velocities in a heated turbulent plane jet. *Phys. Fluids* **19**, 613.

KOVASZNAY, L. S. G., KIBENS, V. & BLACKWELDER, R. F. 1970 Large-scale motions in the intermittent region of a turbulent boundary layer. *J. Fluid Mech.* **41**, 283.

KAWALL, J. G., SHORT, M. & KEFFER, J. F. 1983 A digital technique for the simultaneous measurement of streamwise and lateral velocity in turbulent flows. *J. Fluid Mech.* **133**, 83–112.

LARUE, J. C., DENTON, T. & GIBSON, C. H. 1975 Measurements of high-frequency turbulent temperature. *Rev. Sci. Instrum.* **46**, 757–764.

LARUE, J. C. & LIBBY, P. A. 1974 Temperature fluctuations in the plane turbulent wake. *Phys. Fluids* **17**, 1956–1967.

LECORDIER, J. C., PARANTHOEN, P. & PETIT, C. 1982 The effect of the thermal prong-wire interaction on the response of a cold wire in gaseous flows. *J. Fluid Mech.* **124**, 457–473.

MCMAHON, H. M., HESTER, D. D., & PALFERY, J. G. 1971 Vortex shedding from a turbulent jet into a cross-wind. *J. Fluid Mech.* **48**, 73.

MUCK, K. C. 1980 Comparison of various schemes for the generation of the turbulent intermittency function. *Imperial College Aero. Rep.* 80–03.

MURLIS, J., TSAI, H. M. & BRADSHAW, P. 1982 The structure of turbulent boundary layers at low Reynolds numbers. *J. Fluid Mech.* **122**, 13.

OSWALD, L. J. & KIBENS, V. 1971 Turbulent flow in the wake of a disc. *Tech. Rep.* 002820, University of Michigan, Ann Arbor, Michigan.

PAIZIS, S. T. & SCHWARZ, W. H. 1974 Entrainment rates in turbulent flows. *J. Fluid Mech.* **68**, 297.

PERRY, A. E. & LIM, T. T. 1978 Coherent structures in coflowing jets and wakes. *J. Fluid Mech.* **88**, 451–463.

PERRY, A. E., SMITS, A. J. & CHONG, M. S. 1979 The effects of low frequency phenomena on the calibration of hot-wires. *J. Fluid Mech.* **90**, 415.

PERRY, A. E. & TAN, D. K. M. 1984 Simple three-dimensional vortex motions in coflowing jets and wakes. *J. Fluid Mech.* **141**, 197–231.

RAMSEY, J. W. & GOLDSTEIN, R. J. 1971 An interaction of a heated jet with a deflecting stream. *J. Heat Transfer* **94**, 365.

SCORER, R. S. 1958 *Natural Aerodynamics*, Pergamon.

SREENIVASAN, K. R., ANTONIA, R. A. & STEPHENSON, S. E. 1978 Conditional measurements in a heated turbulent jet. *AIAA J.* **16**, 863.

TOWNSEND, A. A. 1949 The fully developed turbulent wake of a circular cylinder. *Austral. J. Sci. Res.* **2**, 549.

TUTU, N. K. & CHEVRAY, R. 1975 Cross wire anemometry in a high intensity turbulence. *J. Fluid Mech.* **71**, 785.

YULE, A. J. 1978 Large-scale structure in the mixing region of a round jet. *J. Fluid Mech.* **89**, 413.

WALLACE, J. M., ECKELMANN, H. & BRODKEY, R. J. 1972 The wall region in a turbulent shear flow. *J. Fluid Mech.* **54**, 39.

WEIR, A. D., WOOD, D. H. & BRADSHAW, P. 1981 Interacting turbulent shear layers in a plane jet. *J. Fluid Mech.* **107**, 237.

WILLMARTH, W. W. & LU, S. S. 1972 Structure of Reynolds stress near the wall. *J. Fluid Mech.* **55**, 65.

WYGNANSKI, I. & FIEDLER, H. E. 1970 The two-dimensional mixing region. *J. Fluid Mech.* **41**, 327.